SKBF TECHNICAL REPORT
KBS
83-67

Some notes in connection with the studies of final disposal of spent fuel. Part 2

I Neretnieks

Royal Institute of Technology
Stockholm, Sweden May 1983

SVENSK KÄRNBRÄNSLEFÖRSÖRJNING AB / AVDELNING KBS
Swedish Nuclear Fuel Supply Co/Division KBS
MAILING ADDRESS: SKBF/KBS, Box 5864, S-102 48 Stockholm, Sweden
Telephone 08-67 95 40

SOME NOTES IN CONNECTION WITH THE STUDIES OF FINAL DISPOSAL OF SPENT FUEL
Part 2

I Neretnieks
Royal Institute of Technology
Stockholm, Sweden May 1983

A list of other reports published in this series during 1983 is attached at the end of this report. Information on KBS technical reports from 1977-1978 (TR 121), 1979 (TR 79-28), 1980 (TR 80-26), 1981 (TR 81-17) and 1982 (TR 82-28) is available through SKBF/KBS.

SOME NOTES IN CONNECTION WITH THE STUDIES OF FINAL DISPOSAL OF SPENT FUEL

PART 2.

I. Neretnieks
May 1983

This report contains the following "notes" on various subjects related to the Swedish KBS III study.

Neretnieks I.
A note on the transport of hydrogen from a waste canister.

Andersson L., Neretnieks I., Rasmuson A.
Water flow in bedrock. Estimation of influence of transmissive shaft and borehole.

Rasmuson A., Neretnieks I.
A note on the impact of transverse dispersion and "immediately" dissolved radionuclides.

Andersson L., Neretnieks I., Rasmuson A.
Some simple calculations of potential fields in rock mass underneath two typified topographies.

A NOTE ON THE TRANSPORT OF HYDROGEN FROM A WASTE CANISTER

I. Neretnieks
1983-03-31

Summary

Hydrogen produced by radiolysis or corrosion within the backfill can be transported out to the water in the bedrock by three mechanisms.

1. Diffusion through stagnant water in backfill and porous rock matrix.
2. Diffusion through stagnant water in backfill and into the flowing water in the fissured rock.
3. By flow as a gas if the solubility is exceeded.

The first two mechanisms will transport 0.01 - 0.15 moles/year H_2 gas dissolved in water at a pressure of 50 bar.

Transport of hydrogen from the fuel

The hydrogen produced by radiolysis can be transported away by diffusion through the backfill and if the pressure builds up above the hydrostatic pressure by flow through larger pores of the backfill.

An estimate of the transport rate is obtained as follows.

Case 1. Negligible water flow in bedrock

In this case we utilize the diffusional properties from a spherical body into an infinite medium. It can be shown (1) that in the stationary case the transport from a sphere where the concentration at the surface is c_o and the infinite medium has the concentration o at infinity is

$$N = k \cdot A \cdot c_o$$

where A = the surface area of the sphere $4\pi d^2$
k = $2 D_p\varepsilon_p/d$
d = diameter of sphere
$D_p\varepsilon_p$ = effective diffusivity of medium

we get

$$N = 8\pi D_p\varepsilon_p \cdot d \cdot c_o$$

This can be expressed as an equivalent water flow rate Q_{eq} for transporting the dissolved hydrogen gas at concentration c_o

$$N = Q_{eq} \cdot c_o$$

Approximating the 5 m long and 0.75 m diameter canister with a shpere having the same surface area as the canister we get d = 2.0 m.

$D_p\varepsilon_p$ for compacted bentonite has been measured (2) and is

$$3.6\text{-}18 \cdot 10^{-12}\ m^2/s$$

Diffusion measurements of iodide ions and tritiated water in nonfissured granite (3) indicate a formation factor $\delta D/\tau^2 \cdot \varepsilon_p$ of $5\text{-}10 \cdot 10^{-5}$. The diffusivity of hydrogen in water D_V is $10^{-8}\ m^2/s$ (2).

This gives $D_p \varepsilon_p = D_v \frac{\delta D \varepsilon_p}{\tau^2} = 0.5\text{-}1 \cdot 10^{-12}$ m^2/s which is somewhat lower than the diffusivity in the backfill. As the backfill is nearer to the canister and the gradient is the largest there the diffusivity in the backfill will be of somewhat more importance. With a value of $D_p \varepsilon_p = 3.6 \cdot 10^{-12}$ m^2/s we obtain

$$Q_{eq} = 8\pi \cdot D_p \varepsilon_p \cdot d = 5.8 \text{ l/year}$$

with $D_p \varepsilon_p = 1 \cdot 10^{-12}$: $Q_{eq} = 1.6$ l/year

Case 2. Transport by flowing water in the fissures of the rock

In this case we have a flux u_0 in the far field bedrock equal to 1.5 l/m^2·s, a fissure spacing S of 1 fissure/m and fissure widths δ = 0.1 mm with $D_v = 10^{-8}$ and $D_p \varepsilon_p = 3.6 \cdot 10^{-12}$ m^2/s (2). The near field model (4), gives

$$Q_{eq} = 0.5 \text{ l/year.}$$

This model assumes no transport through the matrix of the rock.

Cases 1 and 2 represent entirely different modes of transport. Despite this Q_{eq} is in the same range

$$Q_{eq} = 0.5\text{-}6 \text{ l/year.}$$

At 50 bar the solubility of H_2 in water at 25 °C is about 0.025 mol H_2/l (5). A production of 0.012 - 0.15 mol H_2/year and canister can thus be allowed without exceeding the solubility of hydrogen.

The H_2 production due to α-radiolysis will decrease to such values in the hundred thousand years perspective (6).

Case 3

If the production is larger than that which can be transported away by diffusion, the pressure will build up and finally blow away the water in the pores of the backfill and rock. This has been analysed (7).The hydrogen gas will expel the water from the larger pores of the clay. The analysis indicates that it may be possible to have capillary flow of water in the smaller pores into the clay at the same time as there is gas flow out in the larger pores. It has not been possible as yet to prove that a high hydrogen pressure will prohibit water to enter the fuel and thus stop the radiolysis.

References

1. Bird B., Stewart W., Lightfoot E.
Transport Phenomena. Wiley, 1960, p. 647.

2. Neretnieks I., Skagius K.
Diffusivitetsmätningar av metan och väte i våt lera. 1978. KBS TR 86.

3) Skagius K., Neretnieks I.
Diffusion in crystalline rock of some sorbing and nonsorbing species. 1982. KBS TR 82-12.

4) Neretnieks I.
Leach rates of high-level waste and spent fuel. Limiting rates as determined by backfill and bedrock conditions. Scientific Basis for Nuclear Waste Management V. Symposium Berlin, June 1982, proceedings. North Holland 1982, p. 559-568.

5) Perry R.H., Chilton C.H.
Chemical Engineers´ Handbook, 5th ed.. Mc Graw Hill, 1973, p. 3-97.

6) Christensen H., Bjergbakke E.
Radiolysis of groundwater from spent fuel. KBS TR 82-18. November 1982.

7) Andersson G., Rasmuson A., Neretnieks I.
Migration model for the near field. November 1982.

ROYAL INSTITUTE OF TECHNOLOGY
Department of Chemical Enginnering

WATER FLOW IN BEDROCK

ESTIMATION OF INFLUENCE OF TRANSMISSIVE SHAFT AND BOREHOLE

Lars Andersson
Ivars Neretnieks
Anders Rasmuson

1983-02-11

WATER FLOW IN ROCK

Background

The bedrock, which may appear to be impervious and compact, contains in actuality a system of large and small fractures that permit water transport through the rock mass.

The water content of the bedrock can, under varying hydrostatic pressure conditions, give rise to different flow patterns via boreholes or shafts drilled through the rock.

A case will be dealt with below where an imaginary borehole connects a low point in the terrain with a point in the repository where the hydrostatic pressure is higher than at the mouth of the borehole. The situation may be conceived as having arisen when the area was investigated and a hole was drilled at an angle down from the valley to a point below the high point in the area. (See figure 1.) If the borehole is not sealed, an artesian well may be created.

Fig. 1

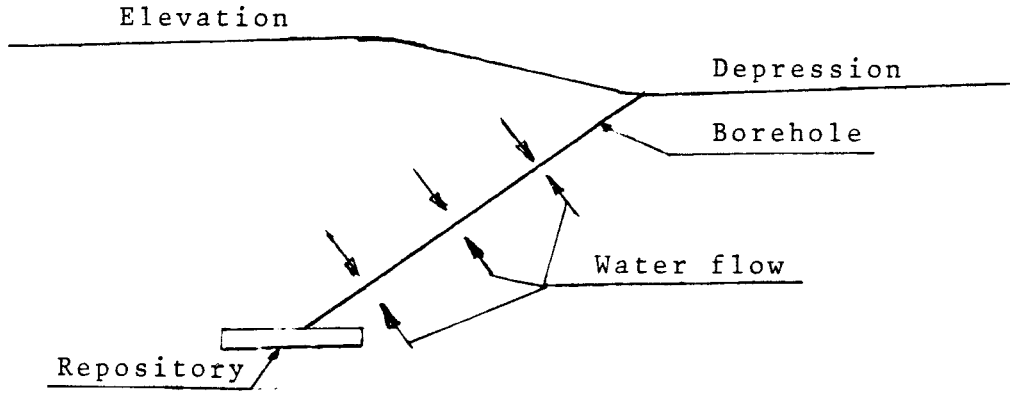

Calculation of water flow

A more or less vertical borehole (shaft) is assumed to be surrounded by a uniformly fractured rock mass saturated with water.

The water level head in the rock mass is higher than the corresponding level in the borehole. This creates a certain hydrostatic pressure in the water in the rock compared to the water in the borehole. The water in the rock strives to flow out into the borehole.

The flow velocity of the water in a section in the rock mass can be expressed as follows:

$$u_o = -k_p \frac{dp}{dz}$$

whereby low flow velocities are assumed (laminar flow).

If a circular slab of the rock perpendicular to the borehole, is considered, the following is obtained for the water flow towards the hole:

$$u_o = -k_p \frac{dp}{dr} \text{ m/s}$$

where

u_o = flow velocity perpendicular to the hole, m/s
k_p = permeability coefficient, m/s
p = static pressurehead in water mass, m H_2O
r = distance from centre of hole, m

The total water flow through a cylindrical surface with a radius of r and a height of l will therefore be:

$$Q = u_o \, 2 \pi r l = -k_p \frac{dp}{dr} \cdot 2 \pi r l$$

The expression can be integrated with respect to r and p in order to obtain a relationship between flow, radius and pressure drop.

In other words, with

$$\frac{dr}{r} = -k_p \, 2 \pi \cdot \frac{l}{Q} dp$$

the following is obtained after integration:

$$\ln \frac{r_y}{r_i} = -k_p \cdot 2 \pi \cdot \frac{l}{Q}(p_y - p_i)$$

where

Q = water flow to borehole m^3/s
p_y = static pressure head at r_y m H_2O
p_i = " " " r_i m H_2O
l = height of slab element m

Relationship between R_y and Q

The following values have been used for approximate calculations with the above integral.

$k_p = 2 \cdot 10^{-9}$, m/s
$l = 5$, m
$P_y - P_i = \Delta p = 12$, m H_2O
$r_i = 0.05$ or 2.5, m

This gives (with $31.54 \cdot 10^6$ s/y):

$$Q = \frac{\Delta P}{\ln \frac{r_y}{r_i}} \cdot 1.9817 \quad m^3/(year, 5m)$$

The corresponding linear water velocity is:

$$u_o = \frac{Q}{r_y} \cdot 0.03183 \quad m/year$$

In order to obtain an idea of the corresponding flow pressure drop, this can be calculated as follows:

$$u_o = -k_p \frac{dp}{dz}$$

or

$$dp = \frac{u_o}{-k_p} dz$$

which, integrated over 10 m, gives

$$\Delta p_{10} = u_o \frac{10}{2 \cdot 10^{-4} \cdot 31.54 \cdot 10^6} = u_o \cdot 158.53 \quad m\ H_2O/\ 10\,m$$

The following is obtained for $r_i = 0.05$ m

r_y	0.25	0.5	1.	2.	5.	10.	20.	50.	100	200. m
Q	14.78	10.33	7.94	6.45	5.16	4.49	3.97	3.44	3.13	2.87 $m^3/y,5m$
r_y/r_i	5	10	20	40	100	200	400	1000	2000	4000
$\ln(r_y/r_i)$	1.61	2.30	3.69	3.69	4.61	5.30	5.99	6.91	7.60	8.29
u_o	1.88	0.66	0.255	0.103	0.033	0.0143	0.0063	0.0022	0.001	0.00046 m/y
Δp_{10}	298.2	104.2	40.06	16.26	5.21	2.26	1.00	.347	.158	0.0723 m H_2O/ /10m

For r_i = 2.5 m:

r_y	5.	10.	20.	50.	100.	200.	500.	1000.	2000. m
Q	34.31	17.15	11.44	7.74	6.45	5.43	4.49	3.97	3.56 $m^3/y,5m$
r_y/r_i	2	4	8	20	40	80	200	400	800
$\ln(r_y/r_i)$	0.69	1.39	2.08	2.99	3.69	4.38	5.30	5.99	6.69
u_o	0.218	0.055	0.018	.0051	.0021	.00086	.00029	.00013	.000057 m/y
Δp_{10}	34.64	8.66	2.89	0.801	0.325	0.137	0.046	0.020	0.090 m H_2O/10 m

The above values thus apply for the pressure drop = 12 m H_2O between r_i and r_y.

However, nothing is said about the pressure drop outside of r_y. Under steady-state conditions, the residual pressure drop outside of r_y should be negligible compared to the pressure drop between r_i and r_y. Some guidance is obtained for evaluating these pressure drop conditions from u_o and $\Delta p/10$ m in the above tables.

For r_i = 0.05 m, r_y can be estimated to be max. 200 m for steady-state conditions. The flow will then be equivalent to max. 3 m^3/year, 5 m.

For r_i = 2.5 m, the corresponding limit may be set = 500 m with Q <=4.5 m^3/ year, 5 m.

In this context, it should be pointed out that values of r_y on the order of 500-5000 m roughly correspond to the distance to major crush zones in the rock. There, the pressure is not affected by the shaft or the borehole, so that larger values of r_y would be misleading to use.

Another way to regard the dependence of flow on r_y and a reasonable estimation of its quantities is presented below.

Limiting value for r_y

If we wish to make a more systematic attempt to estimate a suitable value for r_y, we can define that if the radius r increases by A%, the pressure drop may increase by no more than B% of the pressure drop to r. We then obtain:

$$\ln \frac{r_y(1 + \frac{A}{100})}{r_y} = \Delta p \frac{B}{100} \cdot \frac{1.9817}{Q}$$

which, combined with

$$\ln \frac{r_y}{r_i} = \frac{\Delta p}{Q} 1.9817$$

gives

$$\ln \frac{r_y}{r_i} = \frac{\ln(1 + \frac{A}{100})}{\frac{B}{100}}$$

from which r_y can be solved.

If we decide, for example, that for the area between r_y and r_y + 50% the pressure drop should amount to no more than 5% of the pressure drop to r_y, we obtain

$$A = 50$$
$$B = 5$$

whereby

$$\ln \frac{r_y}{r_i} = \frac{\ln 1.5}{0.05} = 8.1093$$

The water flow is

$$Q = \frac{12}{8.1093} \cdot 1.9817 = 2.93 \quad m^3/(year, 5m)$$

The corresponding values for r_y are

r_i	0.05	2.5	m
r_y	166	8313	m

With r_i = 0.05, the pressure drop is thus 0.6 m H_2O in the approx. 83 m wide ring outside the rock slab with a radius of 166 m. Experience will show if this is a reasonable value.

The value for r_y = 8313 m at r_i = 2.5 m is on the large side, according to the line of reasoning in the preceding section. With a lower value for r_y, Q will increase. For example, r_y = 1 000 m gives about 4 m^3/year.

FLOW VELOCITY IN ROCK

The water's linear mean flow velocity in the fracture system in the rock mass can be calculated as follows:

$$u_e = \frac{Q}{2\pi \cdot r \, l \, e}$$

where

e = porosity in the rock = 0.003

Together with previous constant values, this gives

$$u_e = \frac{Q}{r} \, 10.61 \qquad \text{m/year}$$

The corresponding pressure drop per 10 m is

$$\Delta p_{10} = u_e \cdot 0.4756 \text{ m } H_2O/10 \text{ m}$$

For Q = 2.93 m^3/(year, 5 m), the following is obtained:

r	0.1	0.5	1.0	5.0	10.	50.	100.	200.	500.	1000.	m
u	310.9	62.17	31.09	6.22	3.11	0.622	0.311	0.155	0.0622	0.031	m/year
Δp_{10}	147.8	29.57	14.78	2.96	1.48	0.296	0.148	0.0739	0.0296	0.0148	m H_2O/10 m

Cf. figure 2.

STATIC WATER PRESSURE HEAD

The variation of the static water pressure head with r around a hole is calculated as follows:

$$p = \ln \frac{r_y}{r_i} \cdot \frac{Q}{1.9817}$$

With Q = 2.93 m^3/(year, 5 m), the following is obtained for

r_i = 0.05 m :

r_y	0.05	0.1	0.2	0.5	1.0	2.	5.	10.	20.	50.	100.	200.	500.	m
p	0.0	1.02	2.05	3.40	4.43	5.45	6.81	7.83	8.86	10.21	11.24	12.26	13.62	m H_2O

r_i = 2.5 m :

r_y	2.5	5.	10.	20.	50.	100.	200.	500.	1000.	5000.	m
p	0.0	1.02	2.05	3.07	4.43	5.45	6.45	7.83	8.86	11.24	m H_2O

See also figure 3.

DISCUSSION AND CONCLUSIONS

In the example used above, values on the large side have been used for input quantities in many cases. A pressure head of 12 m assumes that the hydraulic gradient over the region has scarcely been affected at all by the depth, but rather that a local water elevation at the ground surface makes itself felt at a depth of 500 m.

The conductivity used, $2 \cdot 10^{-9}$ m/s, presumes that the repository has been emplaced in average quality rock at this depth. In actuality, the repository site will be selected where the rock is better than average.

In reality, a shaft - even if it is imperfectly backfilled - or a borehole exerts a flow resistance that reduces the available pressure difference at a depth of 500 m.

Taken together, these factors indicate that approx. 5 m^3/(year, 5 m) is the water flow that can be expected to emerge from the repository through a shaft or a borehole. Only this flow can have been contaminated with escaping substances from the repository area. Water that flows in from other parts of the hole dilutes this flow considerably.

FIG. 2. FLOW VELOCITY AROUND A BOREHOLE
Q - 2.93 M3/YEAR, 5 M.

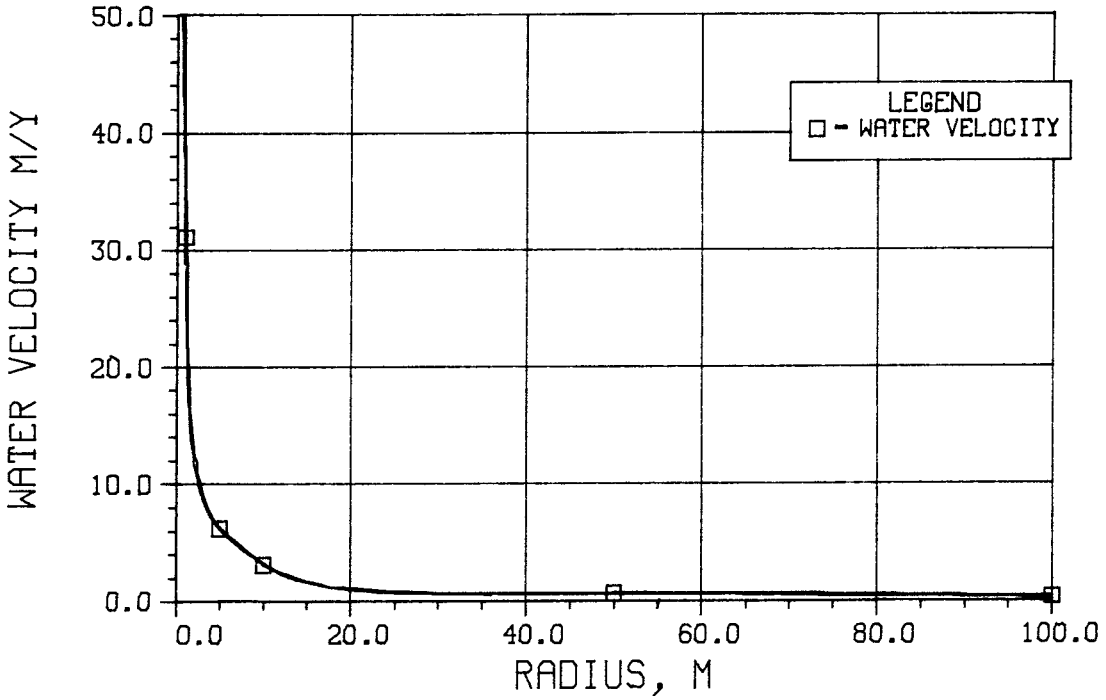

FIG. 3. WATER PRESSURE AROUND THE BOREHOLE
Q - 2.93 M3/YEAR, R - 0.05 OR 2.5 M

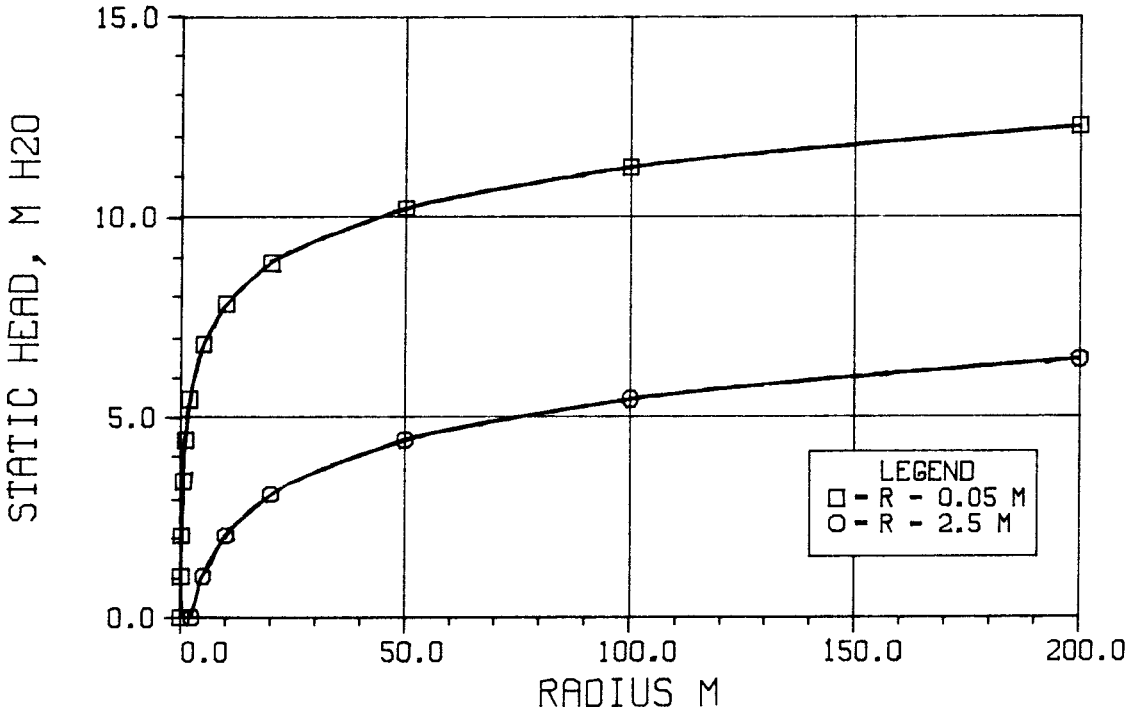

:OYAL INSTITUTE OF TECHNOLOGY
)ept. of Chemical Engineering

A NOTE ON THE IMPACT OF TRANSVERSE DISPERSION AND "IMMEDIATELY" DISSOLVED RADIONUCLIDES

Anders Rasmuson
Ivars Neretnieks

1983-04-08

CONTENTS

SUMMARY

The leach rate of highly soluble species such as iodine has been estimated using a "tank reactor" model. The species are assumed to dissolve in the stagnant pore water (a few thousand liters) in the backfill and to be carried away by the equivalent flowrate in the bedrock (less than 1 liter of water per canister and year). The resulting time constant indicates that half of the species will be leached in a few thousand years.

When a single canister is leached the axial and transverse dispersion will dilute the species in time and space. Sample calculations show that for iodine the concentration 100 m downstream from the canister will be diluted by transverse dispersion to a considerable extent. In the calculated example a factor 1000 was obtained. Axial dispersion is of no importance as the leach time (> 1000 yrs) is much longer than the travel time.

BACKGROUND

In spent fuel some species with high solubility e.g. iodine and cesium have accumulated on the outer sides of the fuel pellets. When water comes in contact with the fuel these species dissolve "immediately" and are quickly leached by the flowing groundwater. The leach rate will be determined by the equivalent flowrate of the water carrying the species away and by the volume of water into which the species are dissolved. The equivalent flowrate of the water is determined by the diffusion in the backfill and in the flowing water. The stagnant volume of water in which the species are dissolved is assumed to be the water volume in the pores of the backfill. This is a fair approximation because the main transport resistance for a dissolved species which moves from the fuel through the backfill and into the moving water in the rock is in the fluid of the fissures in the rock. This means that the species will be rather evenly distributed in the backfill before they diffuse out into the moving water.

When the species move with the water in the rock, axial and transverse dispersion will dilute the species. If the canisters which are leached at any time are far from each other the plumes of the species will not interfere with each other.

TANK REACTOR MODEL OF LEACHING FROM BROKEN CANISTER

In the following it is assumed that the canister is broken and that the radionuclides are dissolved in the water in the clay barrier.

The transport of radionuclides from the water in the clay to the flowing water is modelled as a continuous stirred tank reactor.

Figure 1. Continuous stirred tank reactor.

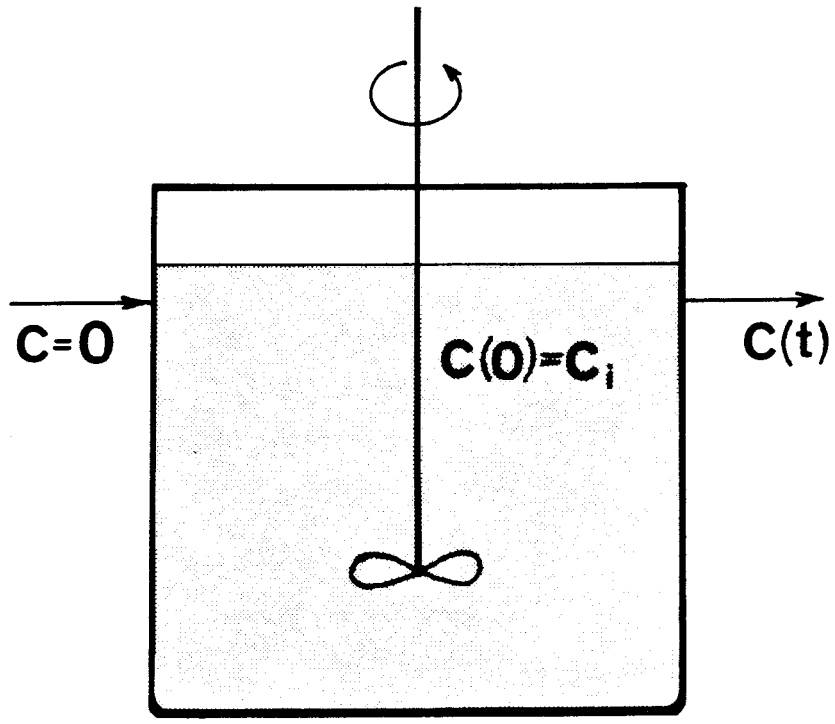

We want to predict C(t). The system is described by:

$$\frac{dC}{dt} + \frac{1}{\tau} C = 0 \qquad (1)$$

with

$$C(0) = C_i \qquad (2)$$

τ is the mean residence time (=V/Q).

The solution of (1) subject to (2) is given by:

$$C = C_i \exp\left(-\frac{t}{\tau}\right) \qquad (3)$$

The "half-live", i.e. the time point for which $C/C_i = 0.5$, is given by:

$$t_{0.5} = \tau \ \ell n\ 2 \qquad (4)$$

The following input data are used:

$$Q = 2.9841 \cdot 10^{-11}\ m^3/s\ (= 0.94\ \ell/yr)$$

$$V = V_{clay} \cdot \varepsilon_{clay} = 5 \cdot \frac{\pi}{4}\left(1.5^2 - 0.75^2\right) \cdot 0.25 = 1.6567\ m^3.$$

Accordingly $\tau = 1.7625 \cdot 10^3$ yrs and $t_{0.5} = 1.2216 \cdot 10^3$ yrs.

THE EFFECT OF LATERAL DISPERSION

Some calculations showing the impact of lateral dispersion on the concentration plume from a single canister are presented.

An analytical solution (Rasmuson, 1981) is used in the calculations. The solution (model) takes into account diffusion and linear sorption in spherical particles, flow and dispersion in the longitudinal direction and lateral dispersion, from a circular disc source.

The solution is given as a function of the following dimensionless parameters:

$$\delta = \frac{3D_p\varepsilon_p}{b^2}\frac{z}{mU_f} \quad , \text{ bed length parameter}$$

$$R = \frac{K}{m} \quad , \text{ distribution ratio}$$

$$Pe_L = \frac{zU_f}{D_L} \quad , \text{ longitudinal Peclet number}$$

$$Pe_T = \frac{a^2U_f}{z\,D_T} \quad , \text{ transverse Peclet number}$$

$$\zeta = \frac{r}{a} \quad , \text{ dimensionless radial distance}$$

$$y = \frac{2D_p\varepsilon_p}{Kb^2}t \quad , \text{ dimensionless time}$$

The data given in Table 1 were used in the calculations. The radius of the disc source, a, is obtained from the projection of the clay barrier perpendicularly to the flow direction (which is assumed to be transverse the cylinder). This surface is then treated as circular.

The lateral dispersion coefficient is assumed to be 10 % of the longitudinal dispersion coefficient. A calculation of the leach time, Δt, was given in the preceding section. The value of K is for a non-sorbing species like iodine. Then $K = \varepsilon_p$.

Parameter	Value	Dimension
$D_p\varepsilon_p$	$5 \cdot 10^{-14}$	m^2/s
b	2.5	m
z	100	m
ε_f	10^{-4}	
U_f	$9.5238 \cdot 10^{-8}$	m/s
K	0.002	
Pe_L	2	
a	1.0925	m
Pe_T	$2.3871 \cdot 10^{-3}, \infty$	
Δt	$1.2216 \cdot 10^{3}, 10^{4}, \infty$	yrs

Table 1: Parameter values used.

From the values given in Table 1 we obtain:

$$q = U_f\varepsilon_f = 0.3 \ l/m^2,yr$$

$$\pi a^2 = 5(1.5-0.75) = 3.75 \ m^2$$

$$\delta = 2.5198 \cdot 10^{-1}$$

$$R = 1.9998 \cdot 10^{1}$$

$$\sigma = \frac{2D_p\varepsilon_p}{Kb^2} = 2.52 \cdot 10^{-4} \ yr^{-1}$$

The calculations are done along the center line, i.e. $\zeta = 0$.

The computer programs LATDIS ($Pe_T < \infty$) and NUCDIF ($Pe_T = \infty$) were used in the calculations.

In Figure 2 the situation for $\Delta t = \infty$ is depicted. The influence of lateral dispersion is clearly demonstrated. For example, the steady-state concentration is nearly three orders of magnitude lower when lateral dispersion is included.

Already from this figure we may draw the conclusion that leach times larger than 10^3 yrs will not have very much effect on the peak height, since the profiles are fully developed. Anyway the cases for which $\Delta t = 1.2216 \cdot 10^3$ and 10^4 yrs are given in Figures 3-4.

The effect of finite leach time is not explicitly included in LATDIS. However, this is easily done by hand subtracting two breakthrough curves with time difference Δt.

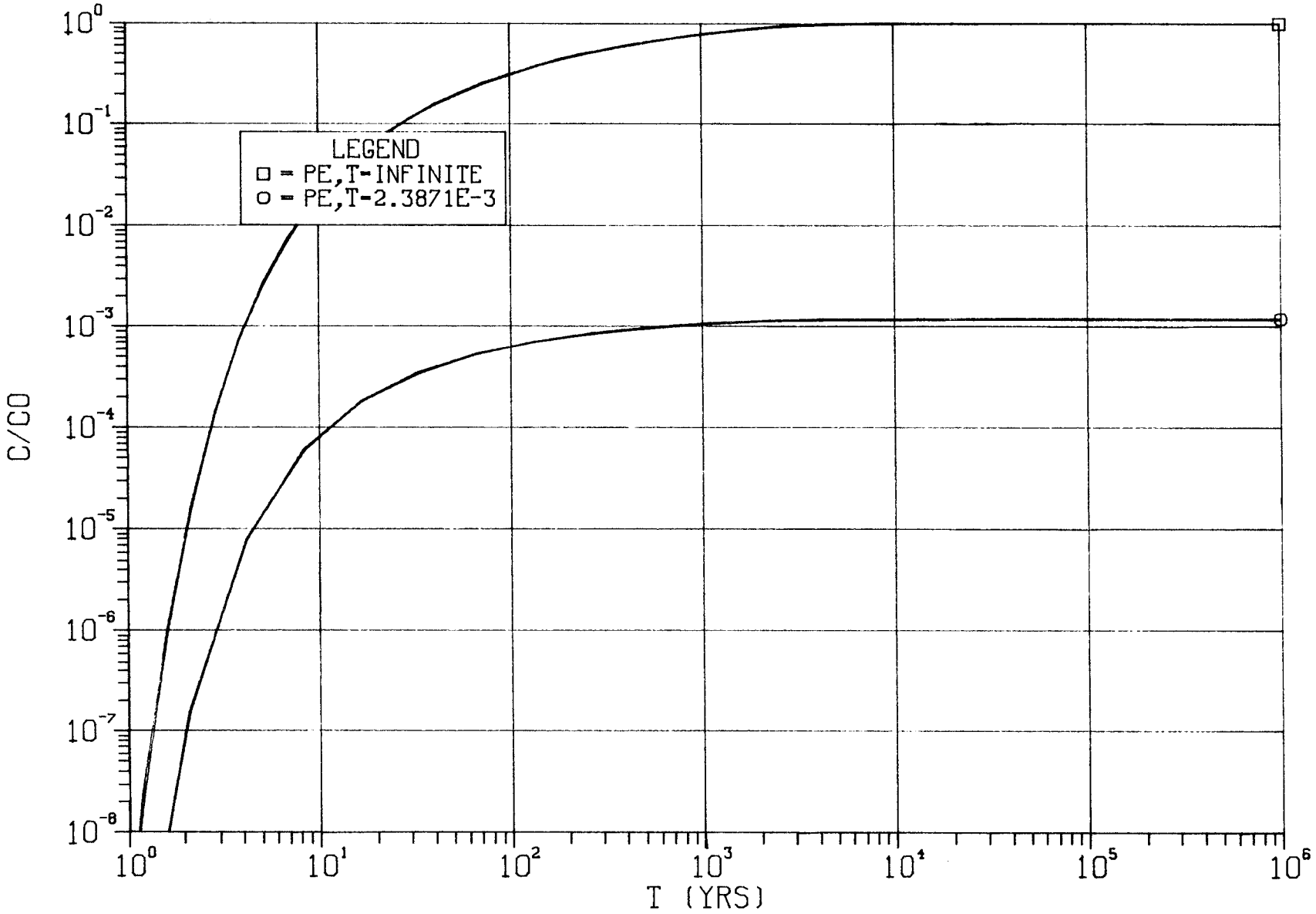
BREAKTHROUGH CURVES
R-1.9998E+1 DELTA-2.5198E-1 PE,L-2.0
TLEAK=INFINITE
LEGEND
□ = PE,T-INFINITE
○ = PE,T-2.3871E-3
C/C0
T (YRS)
10^0
10^-1
10^-2
10^-3
10^-4
10^-5
10^-6
10^-7
10^-8
10^0
10^1
10^2
10^3
10^4
10^5
10^6

Figure 2

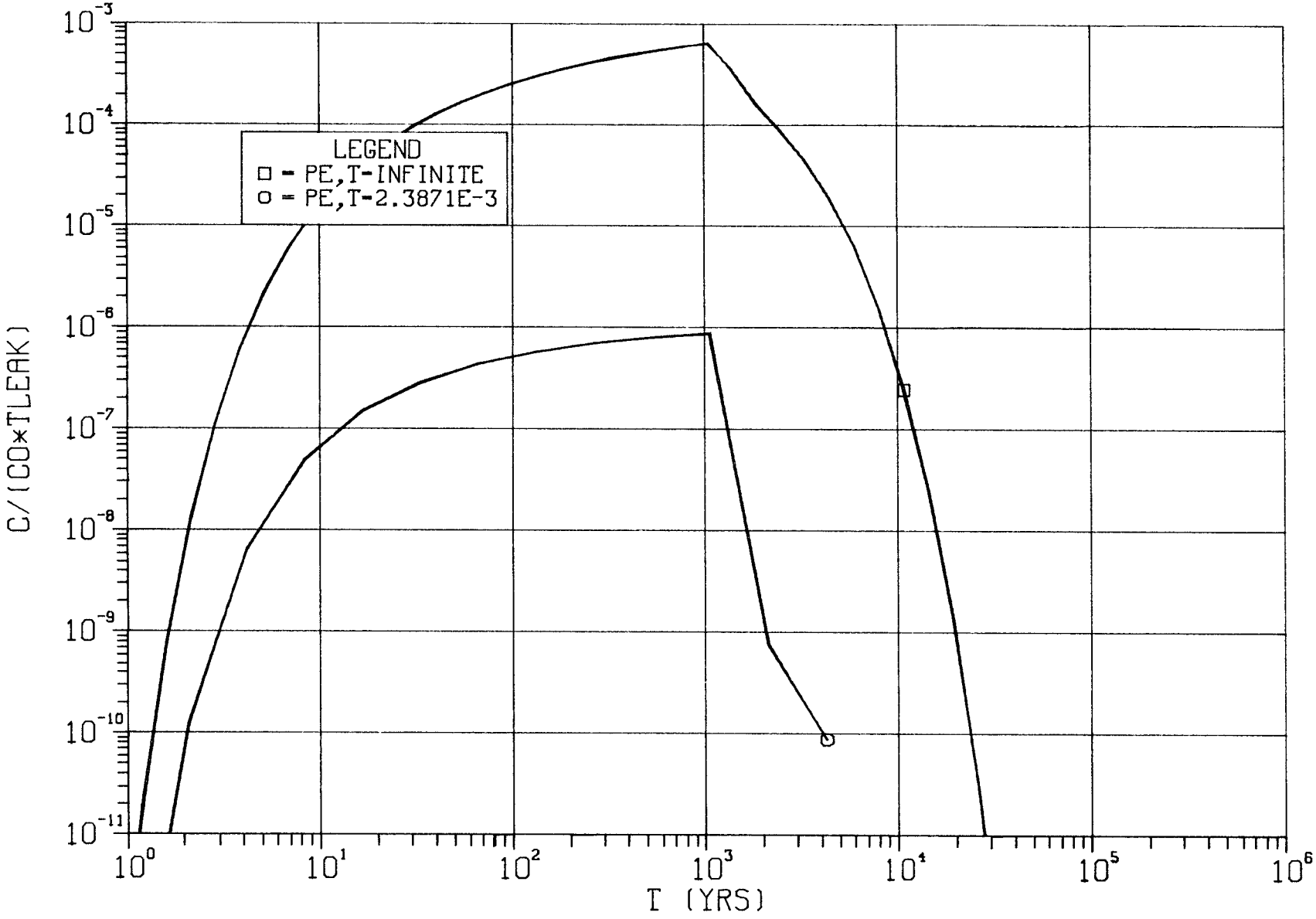
BREAKTHROUGH CURVES
R-1.9998E+1 DELTA-2.5198E-1 PE,L-2.0
TLEAK=1.2216E+3 YRS
LEGEND
□ - PE,T-INFINITE
○ - PE,T-2.3871E-3
C/(CO*TLEAK)
T (YRS)
10^-3
10^-4
10^-5
10^-6
10^-7
10^-8
10^-9
10^-10
10^-11
10^0
10^1
10^2
10^3
10^4
10^5
10^6

Figure 3 3.11

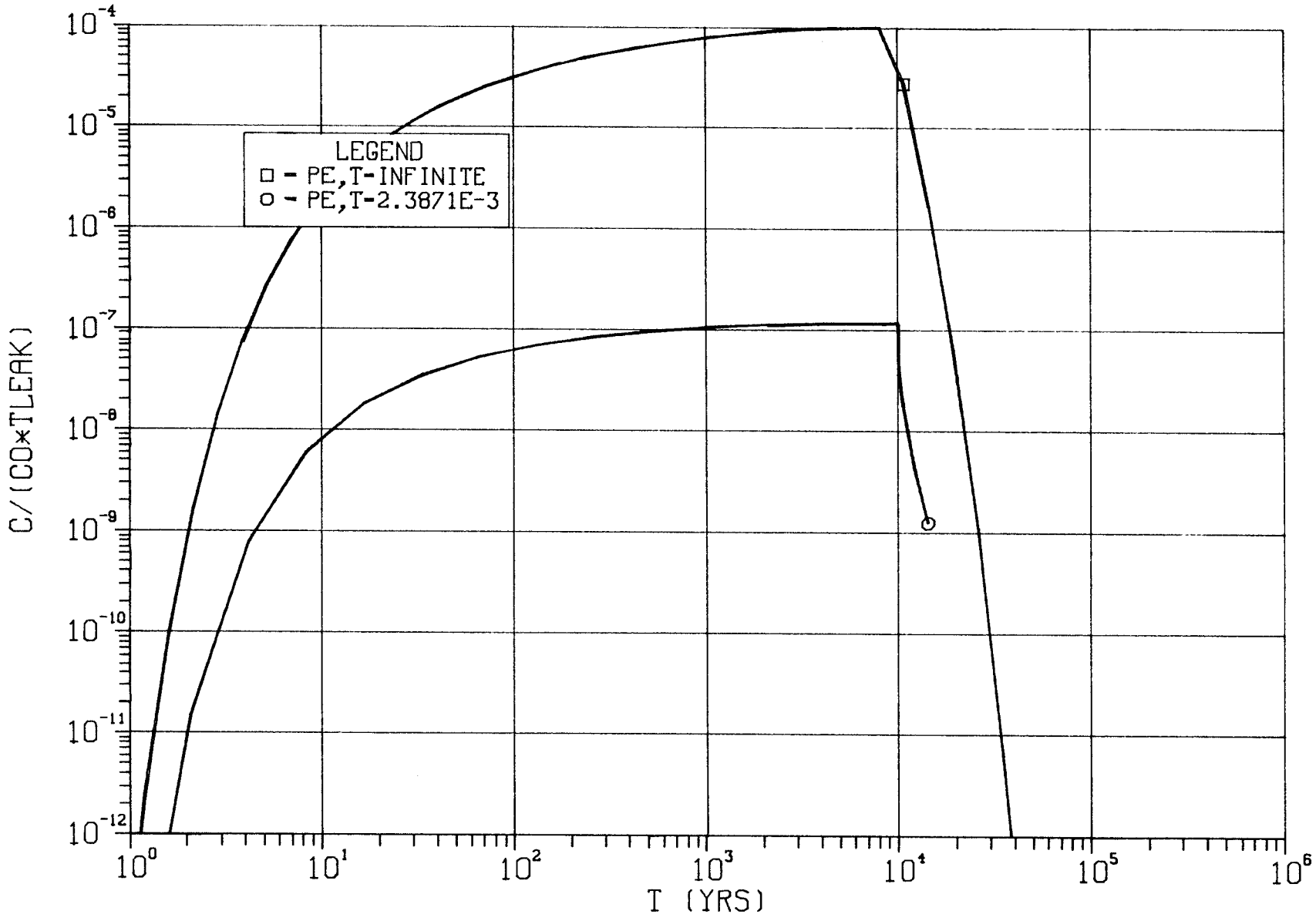
BREAKTHROUGH CURVES
R-1.9998E+1 DELTA-2.5198E-1 PE,L-2.0
TLEAK-1.0E+4 YRS
LEGEND
□ - PE,T-INFINITE
○ - PE,T-2.3871E-3
C/(CO*TLEAK)
T (YRS)
10^-4
10^-5
10^-6
10^-7
10^-8
10^-9
10^-10
10^-11
10^-12
10^0
10^1
10^2
10^3
10^4
10^5
10^6

Figure 4

NOTATION

a	radius of disc surface source	m
b	particle radius	m
C	concentration in water	mol/m^3
C_i	initial concentration	mol/m^3
C_o	inlet concentration in the water	mol/m^3
D_L	longitudinal dispersion coefficient	m^2/s
D_p	diffusivity in water in pores	m^2/s
D_T	transverse dispersion coefficient	m^2/s
K	volume equilibrium constant	m^3/m^3
m	$= \varepsilon_f/(1 - \varepsilon_f)$	
Pe_L	$= zU_f/D_L$, longitudinal Peclet number	
Pe_T	$= a^2U_f/zD_T$, transverse Peclet number	
Q	volumetric flowrate of water	m^3/s
R	$= K/m$, distribution ratio	
r	radial distance	m
t	time	s
$t_{0.5}$	"half-life" of tank reactor	s
Δt	time for dissolution of waste	s
U_f	average velocity of water in fissures	m/s
V	volume of water in clay barrier	m^3
y	$= \frac{2D_p\varepsilon_p}{Kb^2}\,t$, dimensionless time	
z	distance in flow direction	m

Greek letters

δ	$= \frac{3D_p\varepsilon_p}{b^2}\,\frac{z}{mU_f}$, bed length parameter	
ε_f	porosity of fissures	
ε_p	porosity of rock matrix	
ζ	$= r/a$, dimensionless radial distance	
τ	$= V/Q$, mean residence time	s

REFERENCE

Rasmuson A.: Diffusion and sorption in particles and two-dimensional dispersion in a porous medium.
Water Resour. Res. 17, 321-328 (1981).

ROYAL INSTITUTE OF TECHNOLOGY
Department of Chemical Engineering

SOME SIMPLE CALCULATIONS OF POTENTIAL FIELDS IN ROCK MASS UNDERNEATH TWO TYPIFIED TOPOGRAPHIES

Lars Andersson
Ivars Neretnieks
Anders Rasmuson

1983-05-03

CONTENTS

0. SUMMARY

Potential fields and hydraulic gradients have been calculated for some typified topographies.

In one case, a high cylindrical rock mass with a radius of 250 m has been assumed to be surrounded by a 10 m wide fracture zone. The fracture zone has been assigned a conductivity 100 and 10^8 (∞) times higher than that of the rock. The conductivity of the rock decreases with depth. The rock outside the fracture zone is assumed to be impervious. A conical "water mound" with a height of 10 m and a radius of 100 m is placed on the cylinder, which otherwise has a flat water surface. The "water mound" drives the water downward and out to the fracture zone, where it flows upward. The highest gradient at repository depth (approx. 500 m) is about 10^{-3} m H_2O/m.

In another case, the rock mass has been given the form of a 500 m wide vertical slab of infinite extent in the plane of the slab. The same type of fracture zone as in the cylindrical case surrounds the slab on both its vertical sides. A "water ridge" with a height of 10 m and a 200 m base is placed symmetrically on the top surface of the slab. The maximum gradient at a depth of 500 m is now about $7 \cdot 10^{-3}$ m H_2O/m.

An isolated water mound contributes little towards driving the water at great depths. An elongated ridge has a greater influence. In a rock with a hydraulic conductivity of 10^{-10} m/s at a depth of 500 m, the flow in the ridge case would be about 0.02 l/m^2 year.

GROUNDWATER POTENTIALS IN BEDROCK FROM WATER RIDGE AND WATER MOUND

1. BACKGROUND

Spent nuclear fuel is planned to be emplaced in repositories mined in the bedrock. An important factor in evaluating the suitability of such systems is the flow of the groundwater in the bedrock around the repository.

In order for groundwater to flow, potential variations must exist in the water between different areas. Such potential variations in the bedrock can arise due to the fact that the groundwater table follows the upper surface of the bedrock, the ground surface. Below rock elevations saturated with water, a higher potential is obtained in the water in the bedrock compared to the potential under surrounding, lower-lying areas. These potential differences bring about local water movements from areas of higher potential towards areas of lower potential.

The size and direction of the flows are also affected by the bedrock's permeability to water, i.e. its hydraulic conductivity. Variations in the hydraulic conductivity of the bedrock can be expected to influence the pressure head distribution and the corresponding flow.

2. OBJECTIVE

The objective is to try to calculate the distribution of the potential from the water elevation in the horizontal and vertical directions through the bedrock and to determine the influence of fracture zones of differing conductivity on the potential field and the flow pattern.

The calculations are intended to be carried out with the TRUMP program, a numerical computation system based on the integrated finite difference method.

3. GEOMETRIC MODELS

Calculations have been carried out for two alternative geometric models presenting different forms of the water elevation.

In the one model, the water elevation is conceived as a circular conical peak placed in the centre of the top flat surface of a vertical, elongated cylindrical rock body surrounded by a cylindrical fracture zone of differing conductivity (cf. fig. 2, page 9).

In the other model, the water elevation consists of an elongated ridge with flat surfaces placed on the top flat surface of the rock mass. Fracture zones run parallel to the ridge in the rock mass. The longitudinal extent of the ridge and the fracture zones is assumed to be very (infinitely) great compared to the horizontal dimensions in the perpendicular section through the ridge in the rock mass.

For both models, the bedrock is assumed to be uniformly fractured (constant conductivity) in the horizontal direction but variably fractured in the vertical direction.

The fracture zone is assumed to have differing, greater conductivity than the rock mass.

The entire rock mass, including elevation and fracture zone, is assumed to be saturated with water. The top water surface (i.e. the water table) follows the surface of the ground, i.e. the rock elevation and surrounding, horizontal surfaces.

The bedrock outside the fracture zone is assumed to have considerably lower hydraulic conductivity than the fracture zone (= impervious wall).

4. MATHEMATICAL MODEL

The distribution of the groundwater potential in the rock mass from a water elevation is assumed to be able to be represented by the equation

$$\nabla \cdot (K_p \nabla \phi) = 0$$

for both geometric models.

The potential field underneath the water ridge can, if infinite length is assumed, be expressed by a two-dimensional, elliptical differential equation as follows:

$$K_p \frac{\partial^2 p}{\partial \ell^2} + \frac{\partial}{\partial z} \left(K_p \frac{\partial p}{\partial z}\right) = 0$$

where ℓ and z stand for the geometric coordinates in the horizontal and vertical directions, respectively, and K_p is a function of z.

If the rock is regarded as pseudohomogeneous (i.e. K_p is constant), the Laplace equation is obtained:

$$\frac{\partial^2 p}{\partial \ell^2} + \frac{\partial^2 p}{\partial z^2} = 0$$

The corresponding relationship for the cylindrical model with conical water mound is (with $K_p(z)$):

$$K_p \frac{1}{r} \frac{\partial}{\partial r} \left(r \frac{\partial p}{\partial r}\right) + \frac{\partial}{\partial z} \left(K_p \frac{\partial p}{\partial z}\right) = 0$$

or in differentiated form and with pseudohomogeneous rock:

$$\frac{\partial^2 p}{\partial r^2} + \frac{1}{r} \frac{\partial p}{\partial r} + \frac{\partial^2 p}{\partial z^2} = 0$$

where r is the horizontal, radial coordinate.

The hydraulic conductivity is assumed to vary with depth according to:

$$K_p = 10^{-6\left(1 + \frac{z}{1000}\right)} \qquad \text{m/s (z in m)}$$

The variation of conductivity with rock depth is entered into the TRUMP program via the material specification, where the conductivity is specified for each element.

5. BOUNDARY CONDITIONS

The potential from the water elevation on the top surface is expressed for the water ridge:

$$p = 0.1 \ \ell_o \left(1 - \frac{\ell}{\ell_o}\right) \qquad \text{m } H_2O$$

where

ℓ_o = half the width of the ridge in m

the water mound :

$$p = 0.1\ r_o\ (1 - \frac{r}{r_o}) \qquad m\ H_2O$$

where

r_o = the radius of the water mound in m.

In addition, the following applies in both geometric models for the flat surface outside the water elevation on the top surface:

$$p = 0.0 \qquad m\ H_2O$$

The following applies for the surface of the bedrock against the fracture zones:

$$|K_p \frac{\partial p}{\partial \ell}|_{rock} = |K_p \frac{\partial p}{\partial \ell}|_{fracture}$$

An impervious boundary is assumed to exist at the interface between the fracture zone and the surrounding rock.

At the bottom flat surface of the rock mass, it is assumed that the influence of the water elevation on the potential field has ceased or that

$$\frac{\partial p}{\partial z} = 0.$$

In order for this boundary condition to be realized, a sufficiently great rock depth must be chosen.

Symmetrical conditions are assumed to prevail along the centre plane (the centre axis), i.e.

$$\frac{\partial p}{\partial \ell} = 0 \quad (\frac{\partial p}{\partial r} = 0)$$

As a starting value, p is set equal to 0. Another value may also be chosen (e.g. p = 1), since the calculated pressure field should contain the same values, regardless of the starting values, under steady-state conditions.

6. TRUMP Program

The TRUMP program is, as mentioned above, a numerical method based on the integrated finite difference method for solving general, non-linear, parabolic or elliptical differential equations.

With TRUMP, steady-state and unsteady-state processes can be computed for geometric models with one, two or three dimensions with rectangular, cylindrical or spherical symmetry. Other asymmetric geometries and dimensions can also be treated.

Time-independent problems are solved as if they were time-dependent, but the demand on accuracy during the time-dependent phase is set low.

The TRUMP program was originally developed to solve thermal diffusion and flow problems, but the program can also be used for other computation problems, provided that the same mathematical model applies as for the thermal processes.

An example of the division of a vertical section through the rock mass into elements in the horizontal and vertical direction from the centre is shown in figure 3. A denser network of elements (smaller elements) has been chosen for the area underneath the water elevation down to a depth of about 600-700 m than for other areas. It is in this area that the large changes of the potential field can be expected. The network applies for both the rectangular and the cylindrical models.

In order to ensure that the bottom surface of the rock model will not influence the conditions around 500 m, it has been located at the 3 000 m level. The TRUMP program will regard the rock as insulated on the outside, i.e. with

$$\partial p/\partial z = 0.$$

In using TRUMP, numerous input data must be entered for the problem at hand. All elements (element nodes) must be numbered and dimensioned, as well as node distance to and dimensions of the contact surfaces between the elements.

Conductivity is assumed in the above model to vary with depth, and the pseudohomogeneous condition is fulfilled by defining each element layer as a separate kind of material.

A special program has been put together to design the TRUMP program's input data file for the geometric models described above.

7. GRAPHIC DIAGRAMS

Special programs have also been prepared to design plotting files for graphic diagrams in accordance with the DISSPLA system valid for data calculated according to the TRUMP program.

Each potential field that has been calculated with the TRUMP program is depicted in a diagram system consisting of five different types of diagram.

One diagram shows potential values in the horizontal direction for different levels.

Two diagrams show potential gradients in the horizontal and vertical direction as a function of horizontal coordinate at different levels. These gradient values are of importance for evaluating and calculating the water flow in the rock mass.

The fourth diagram shows the potential field in a 3D diagram, i.e. a diagram with three axes with pressure as a function of the horizontal and vertical coordinates.

The fifth diagram is a contour diagram for the pressure field. This type of diagram is an alternative to the 3D diagram and provides more detailed information on the potential field.

8. MODEL DIMENSIONS

Calculations have thus far been carried out for four different cases. The potential fields have been calculated for the two geometric models described above with two different relative conductivities in the fracture zone.

For both geometric models, the potential field has been calculated for a two-dimensional section through the rock with the following dimensions:

250 x 3100 m (rock mass) + 10 x 3100 m (fracture zone).

These dimensions apply from the centreline out to and including the fracture zone.

The water elevation (ridge or mound) has the following dimensions (counting from the centre):

10 x 100 m with a triangular, vertical section.

The vertical section through the rock mass is divided into an element field with the following dimensions in the horizontal direction:

1 + 9 + 9 x 10 + 5 x 25 + 24 + 1 + 10 m

in the vertical direction:

0 + 9 x 50 + 45 + 5 + 4 x 50 + 7 x 200 + 2 x 500 m.

Thus, in the horizontal direction, the elements closest to the centre are 1 m wide, the next 9 m etc. out to the fracture zone, where the elements closest to this zone are 1 m wide. The first eleven elements correspond to the bottom surface of the water elevation.

In the vertical direction, the elements at the top consist of "zero volume" elements according to the TRUMP conditions for interfacing with the boundary conditions from the water elevation.

At the 500 m level, a 5 m high row of elements represents the location of the repository.

The element dimension perpendicular to the vertical section has been set equal to 1 m in the rectangular model.

In the circular model, TRUMP uses annular elements and surfaces.

In the calculations, hydraulic conductivity in the fracture zone has been set to 10^2 and 10^8 times the conductivity of the rock mass at the same level.

Some characteristic geometric data that apply for the calculation case have been given in the third column in the diagrams.

L (WR) = horizontal length from centre for water ridge
R (WH) = radius for water mound
L (F) = distance centre - fracture zone
R (F) = radius to fracture zone
Z (M) = maximum depth level
K_p (F) = hydraulic conductivity in fracture zone
K_p = hydraulic conductivity in rock mass
E+2 = factor in powers of ten for fracture conductivity (E+2 = 100)

9. CALCULATION RESULTS

The calculation results for the four cases are plotted in the 20 appended diagrams Nos. 1-20.

The diagrams are arranged with five diagrams for each case in sequence in the following order:

water ridge with low fracture conductivity
water ridge with high fracture conductivity
water mound with low fracture conductivity
water mound with high fracture conductivity

The diagrams for the potential field values contain data for seven different levels between 25 and 675 m.

It can be seen here that, with low conductivity in the fracture, the potential in the fracture increases with increasing depth, which means upward flow in the fracture. This also applies to the potential field region nearest the fracture zone.

These diagrams also show the great difference between the potential field underneath the water mound and the water ridge with the same dimension. 5-10 times higher values are obtained underneath the water ridge.

At high fracture conductivity, the potential field nearest the fracture decreases, especially in the region 50 m from the fracture.

Underneath the actual water elevation, however, the potential field does not seem to be affected so much by the conductivity of the fracture.

The diagrams for the potential gradients show horizontal and vertical potential field gradients around the 500 m level.

The horizontal gradients reach their maximum at the fracture, while the vertical gradients are greatest some distance in. If the total gradient for a level is calculated, its absolute value is relatively constant but with varying direction (from vertical to horizontal). This is especially true underneath the water mound.

The gradients are considerably greater underneath the water ridge than underneath the mound (5-10 times), as is the difference between the vertical and horizontal directions.

The 3D diagrams provide overall pictures of the appearance and size of the pressure field for levels down to 600 m.

Unfortunately, the self-graduating DISSPLA Functions have widened the field to 300 m in the horizontal direction, which does not correspond to actual conditions.

Nevertheless, the diagrams clearly show the difference between the potential field underneath the water mound and the one underneath the water ridge.

The diagrams also show a potential field drop just under the zero level outside the water elevation area. Here, there is an upward flow of the water from the water elevation.

The contour diagrams show potential curves between the 300 and 700 m level. The figures in the curves give the pressure head in m H_2O.

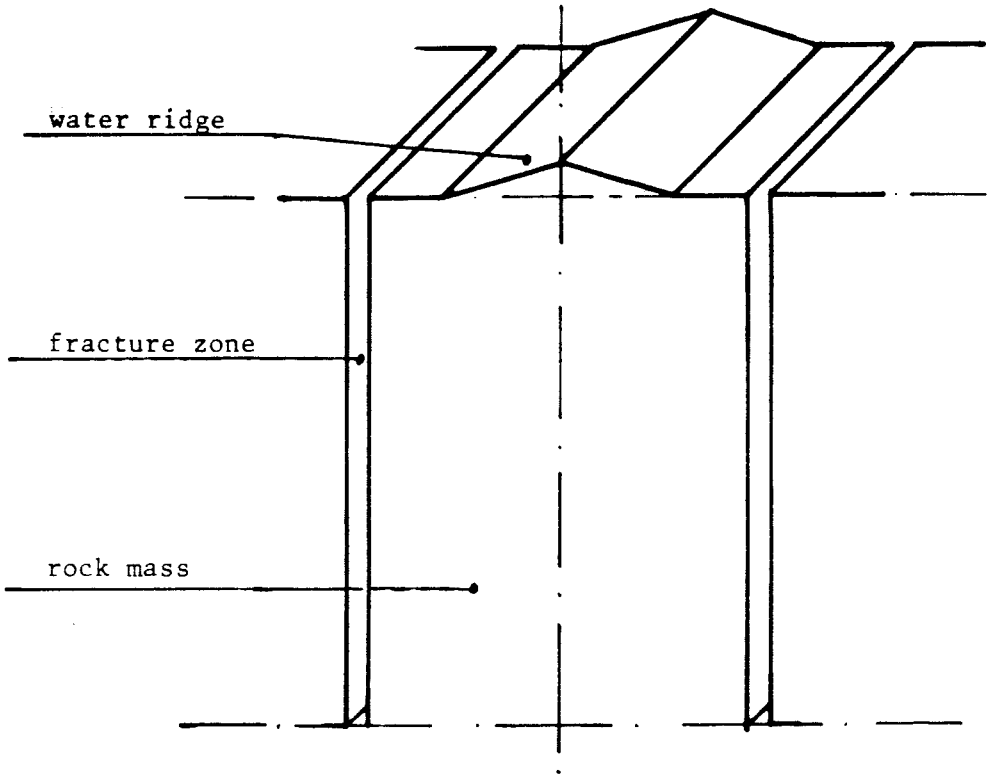

FIG. 1 GEOMETRIC MODEL WITH WATER RIDGE.

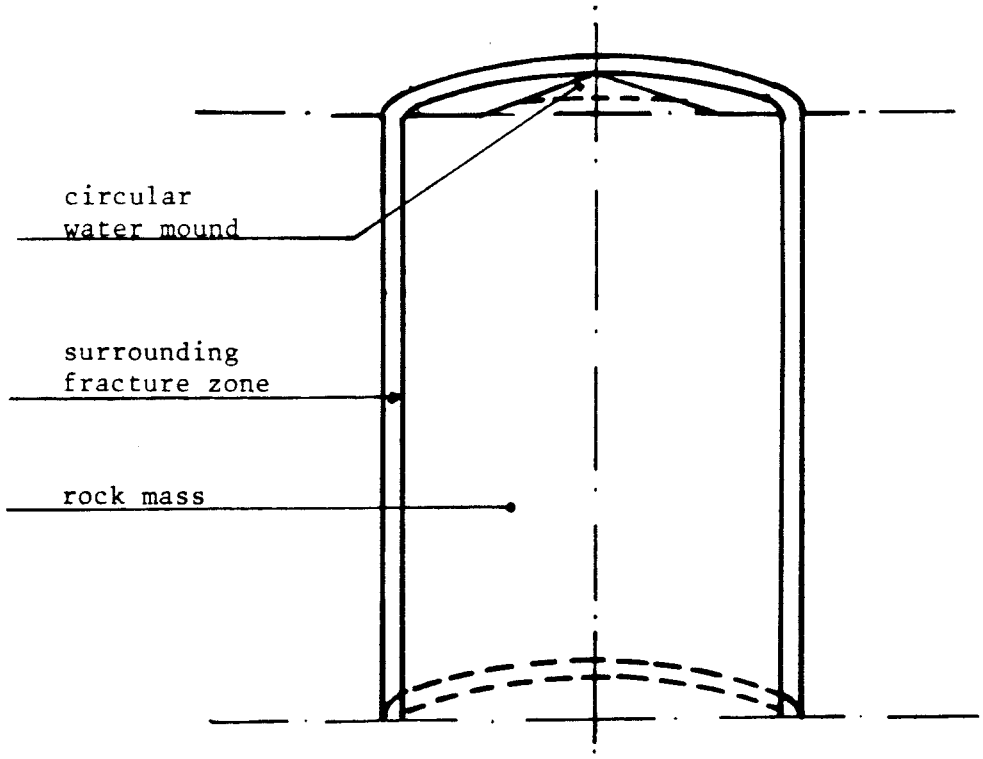

FIG. 2 GEOMETRIC MODEL WITH WATER MOUND.

POTENTIAL FIELD FROM WATER ELEVATION

Element network for TRUMP calculations.

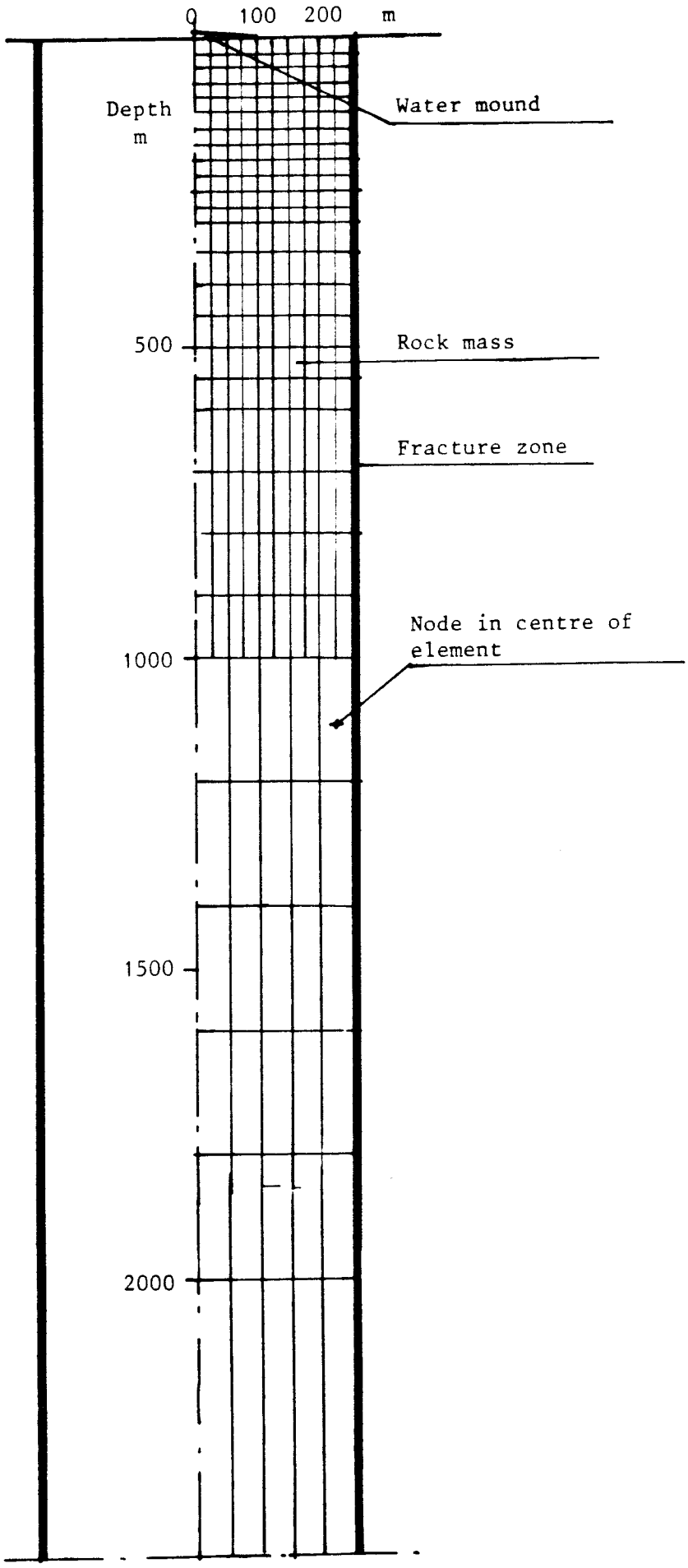

Fig. 3

Example of element network for TRUMP calculations

Scale 1:10 000

(Applies for both geometric models)

DIAGRAM NO: 1

POTENTIAL FIELD FROM WATER RIDGE.

WATER RIDGE POTENTIALS AT VARIOUS LEVELS.

L(WR)-100 M, L(F)-250 M, Z(M)-3100 M, KP(F)-KP*(E+2)

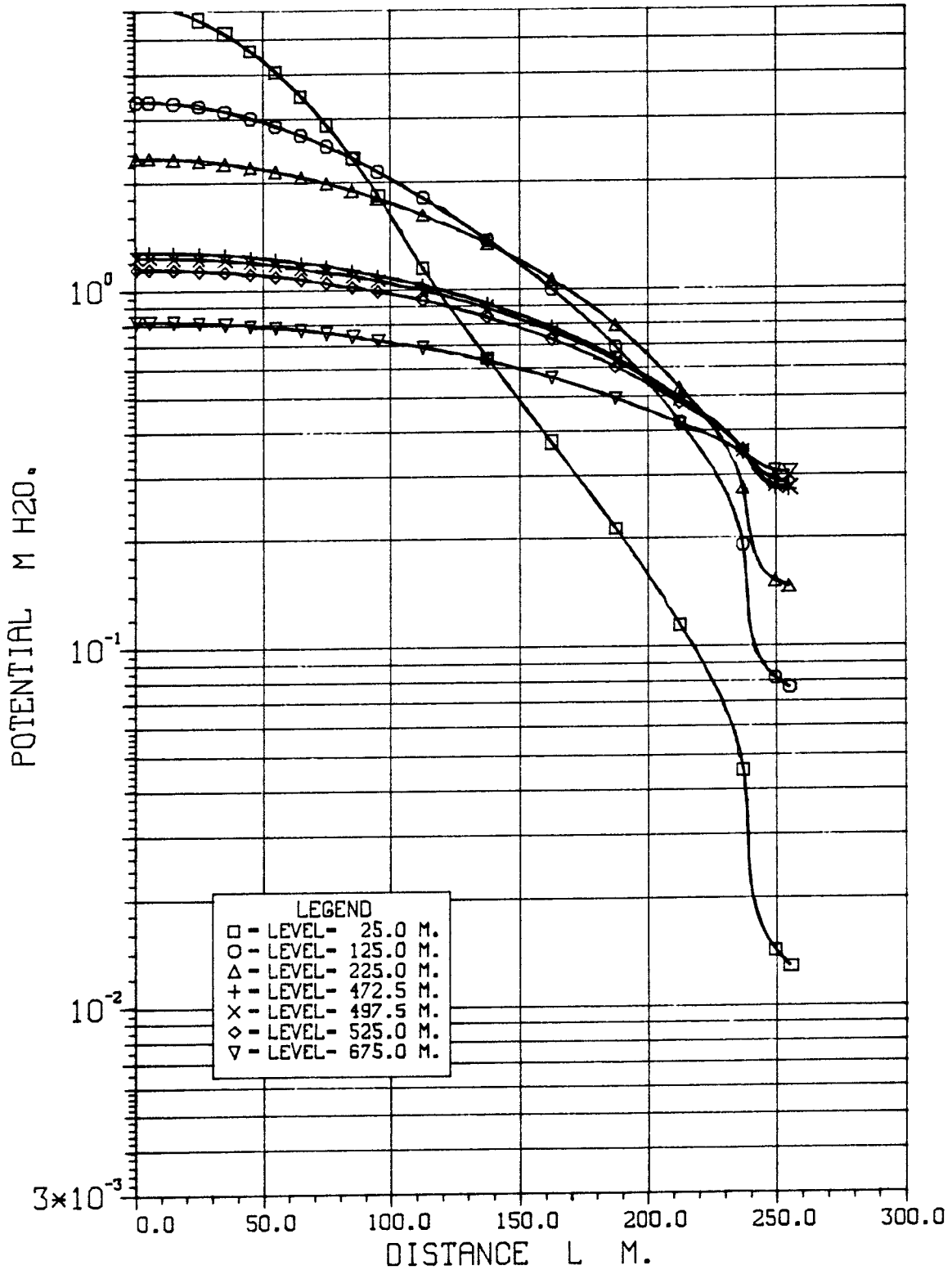

POTENTIAL FIELD FROM WATER RIDGE.

HORISONTAL POTENTIAL GRADIENTS AT VARIOUS LEVELS.

L(WR)-100 M, L(F)-250 M, Z(M)-3100 M, KP(F)-KP×(E+2)

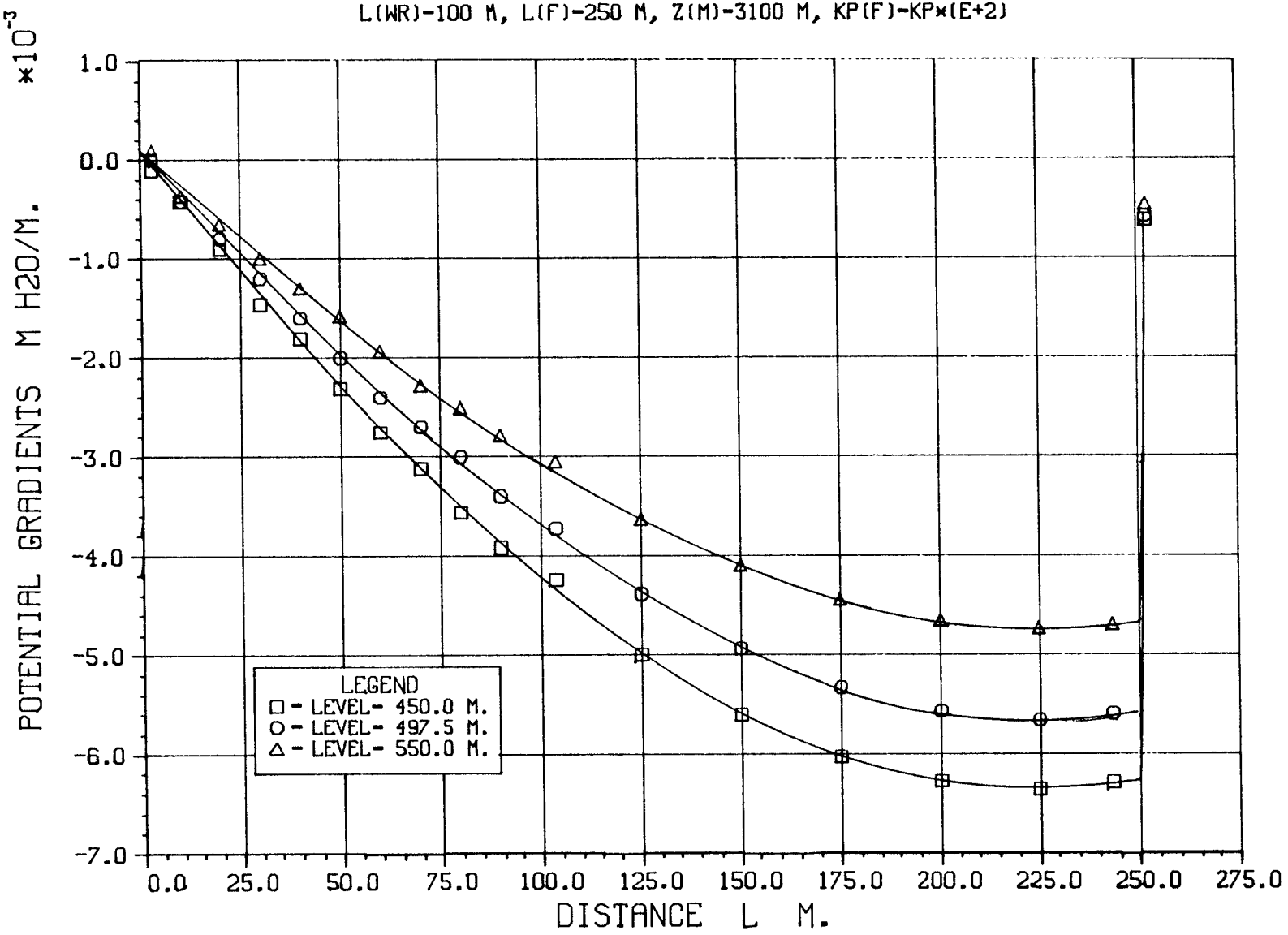

DIAGRAM NO: 2

POTENTIAL FIELD FROM WATER RIDGE.

VERTICAL POTENTIAL GRADIENTS AT VARIOUS LEVELS.

L(WR)-100 M, L(F)-250 M, Z(M)-3100 M, KP(F)-KP*(E+2)

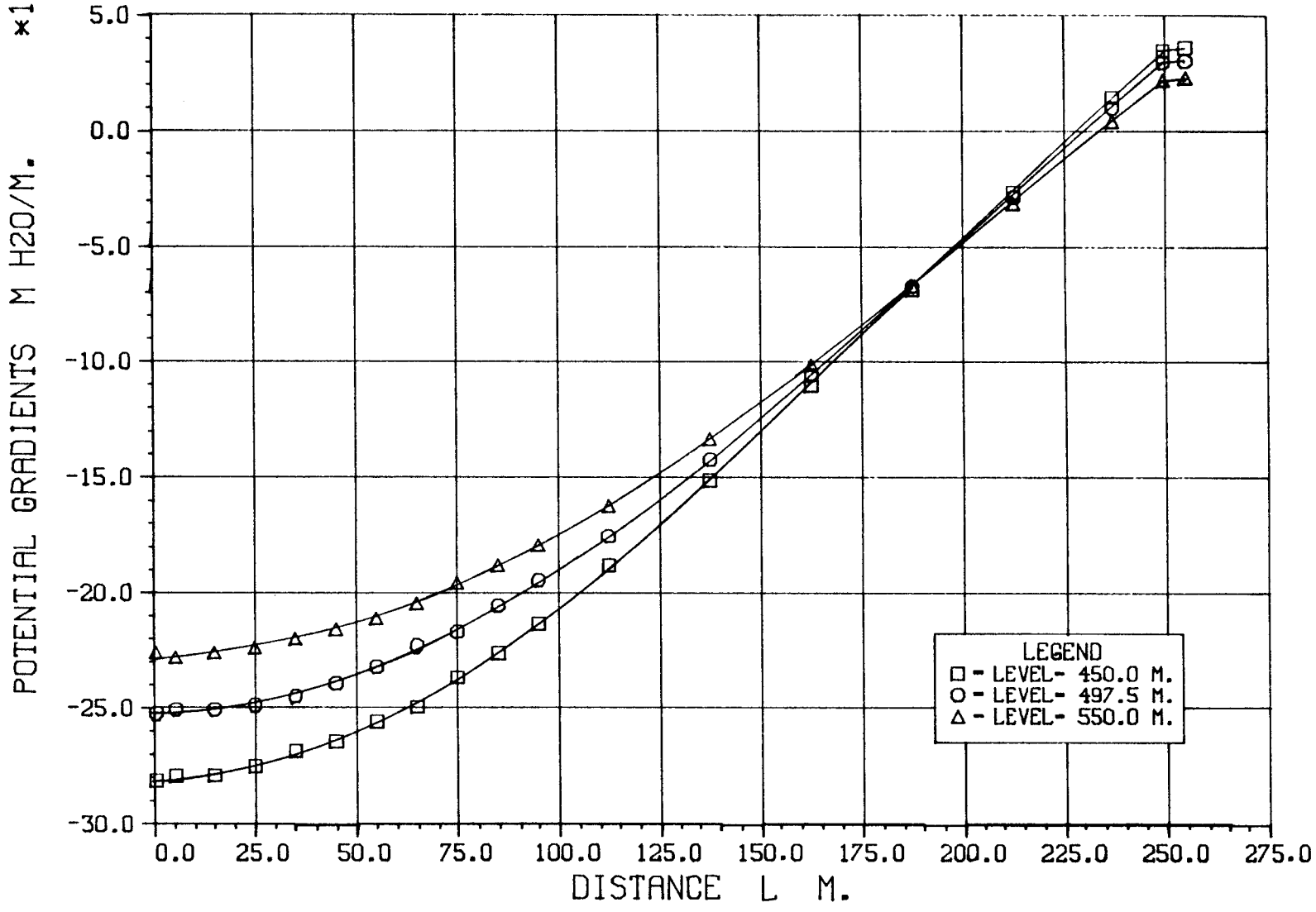

DIAGRAM NO: 3

DIAGRAM NO: 4

POTENTIAL FIELD FROM WATER RIDGE.

3D-DIAGRAM FOR POTENTIAL FIELD.

L(WR)-100 M, L(F)-250 M, Z(M)-3100 M, KP(F)-KP*(E+2)

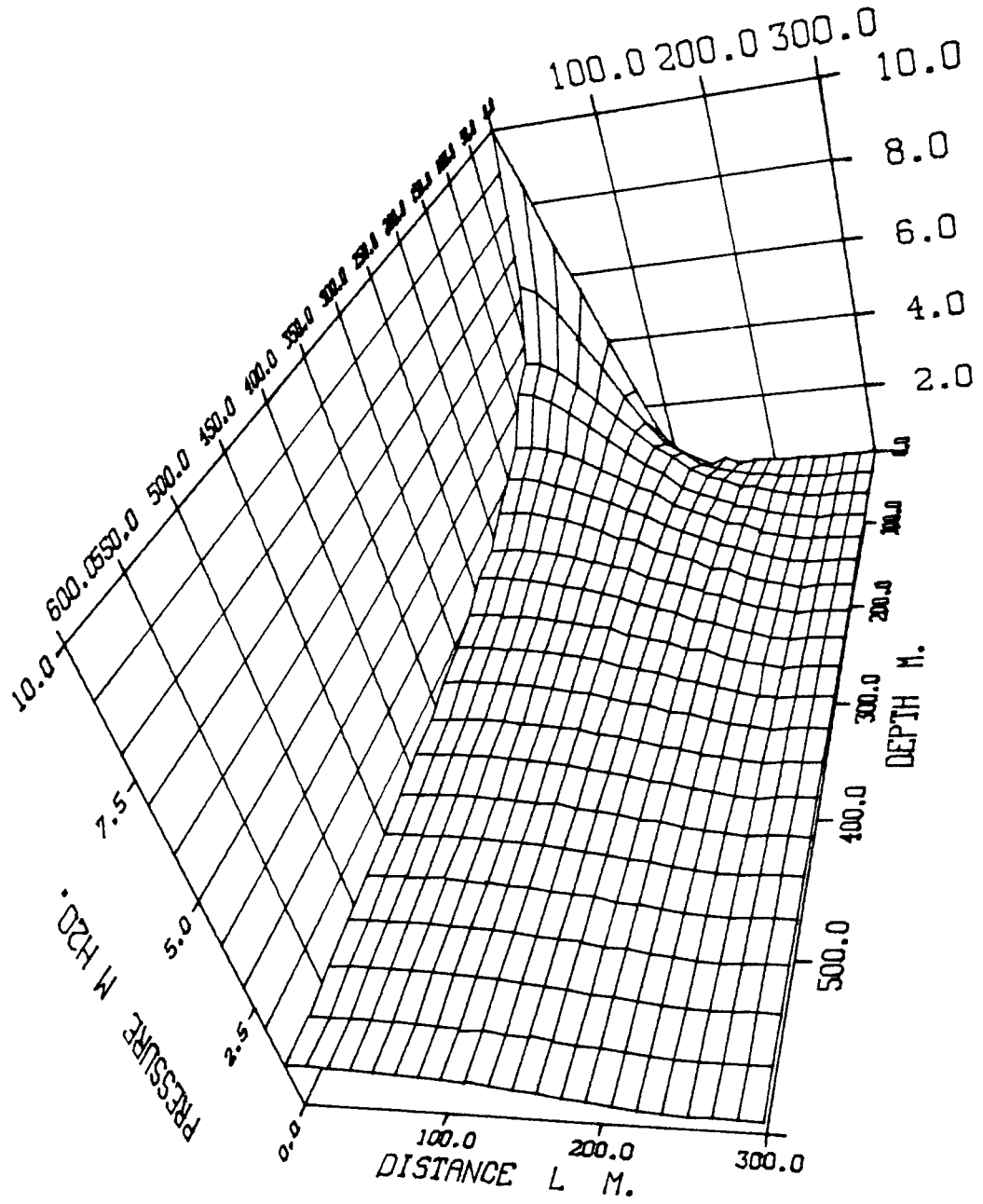

POTENTIAL FIELD FROM WATER RIDGE.

CONTOUR DIAGRAM FOR POTENTIAL FIELD.

L(WR)-100 M, L(F)-250 M, Z(M)-3100 M, KP(F)-KP*(E+2)

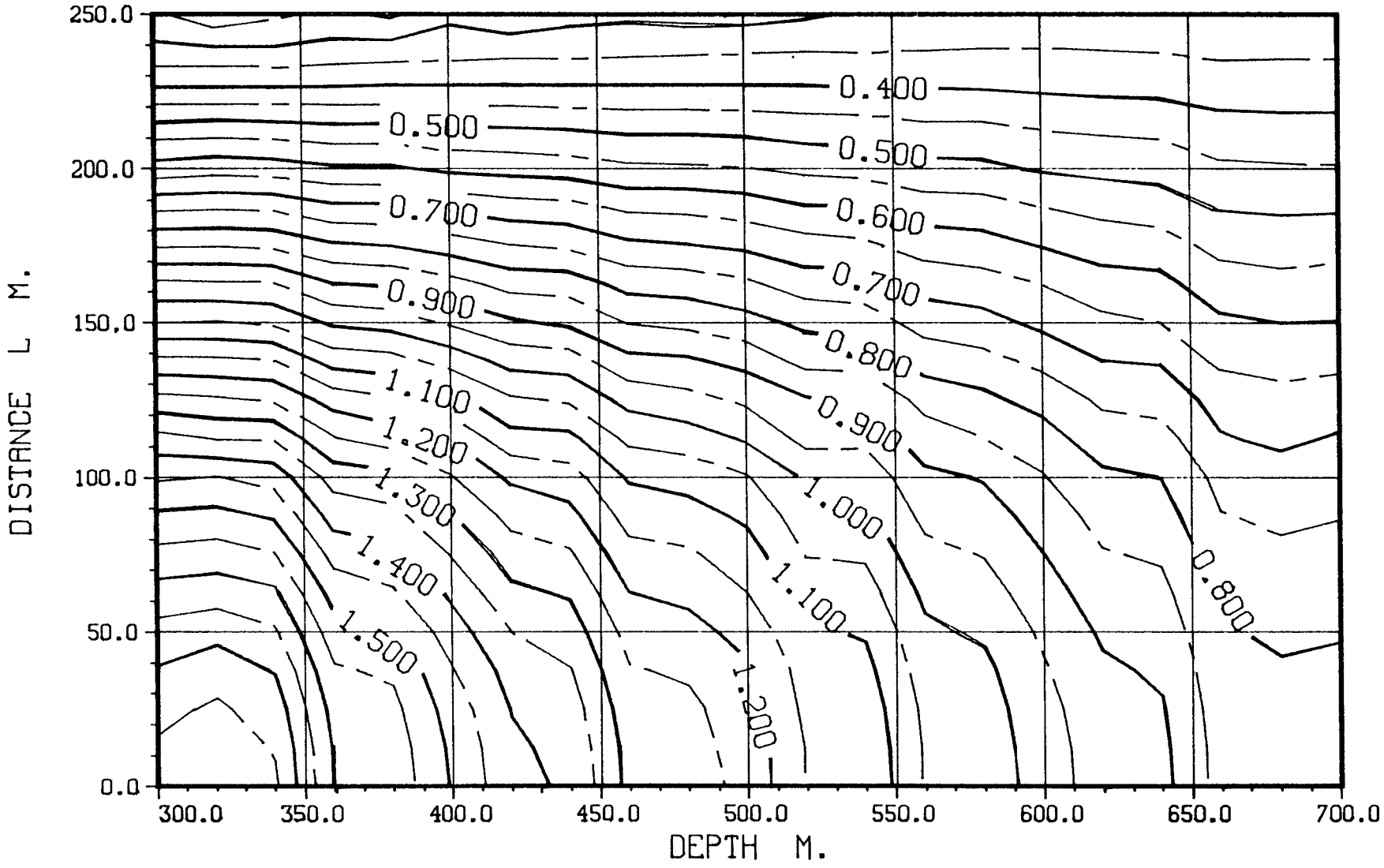

DIAGRAM NO: 5

DIAGRAM NO: 6

POTENTIAL FIELD FROM WATER RIDGE.

WATER RIDGE POTENTIALS AT VARIOUS LEVELS.

L(WR)-100 M, L(F)-250 M, Z(M)-3100 M, KP(F)-KP*(E+8)

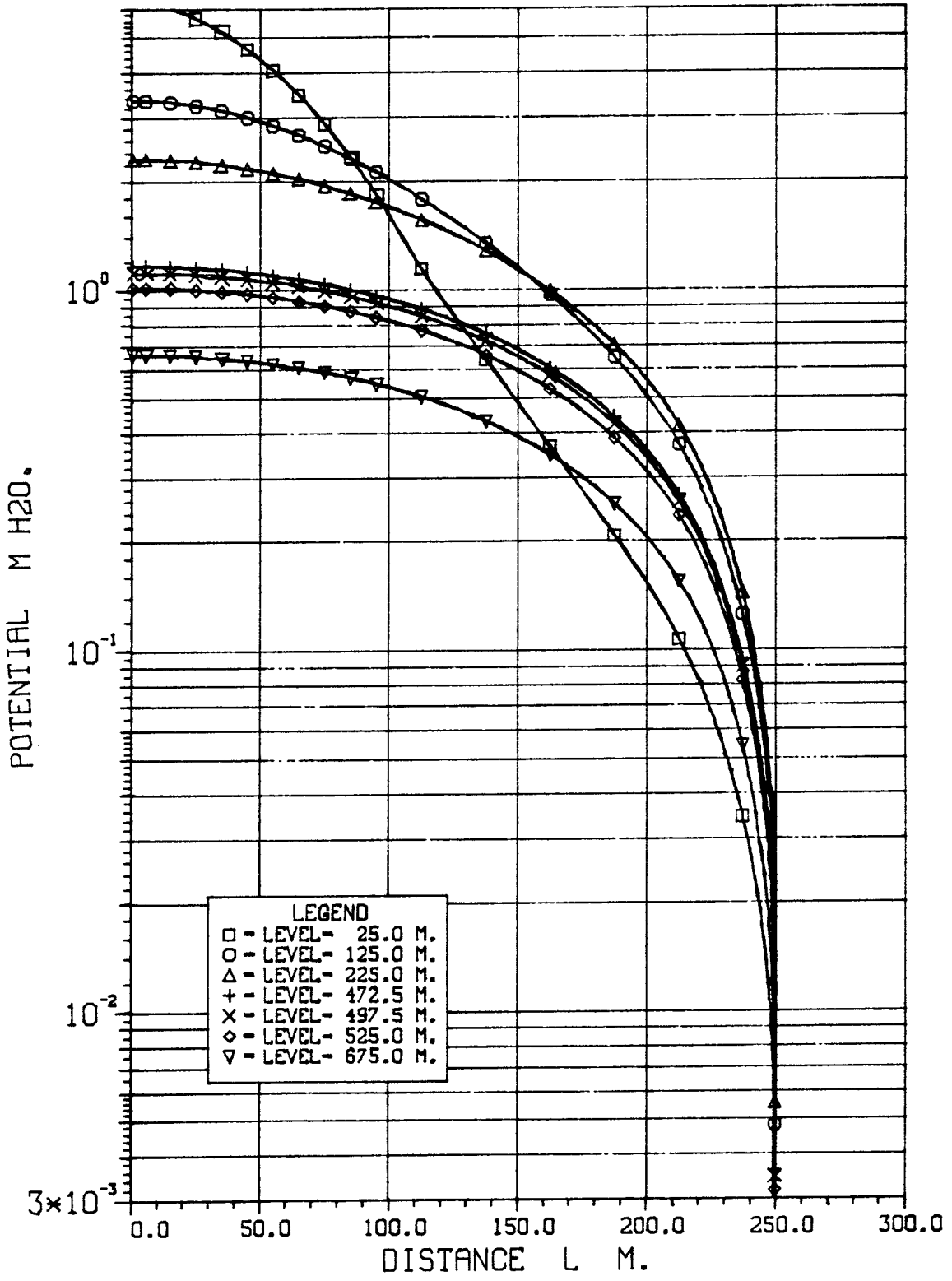

POTENTIAL FIELD FROM WATER RIDGE.

HORISONTAL POTENTIAL GRADIENTS AT VARIOUS LEVELS.

L(WR)-100 M, L(F)-250 M, Z(M)-3100 M, KP(F)-KP*(E+8)

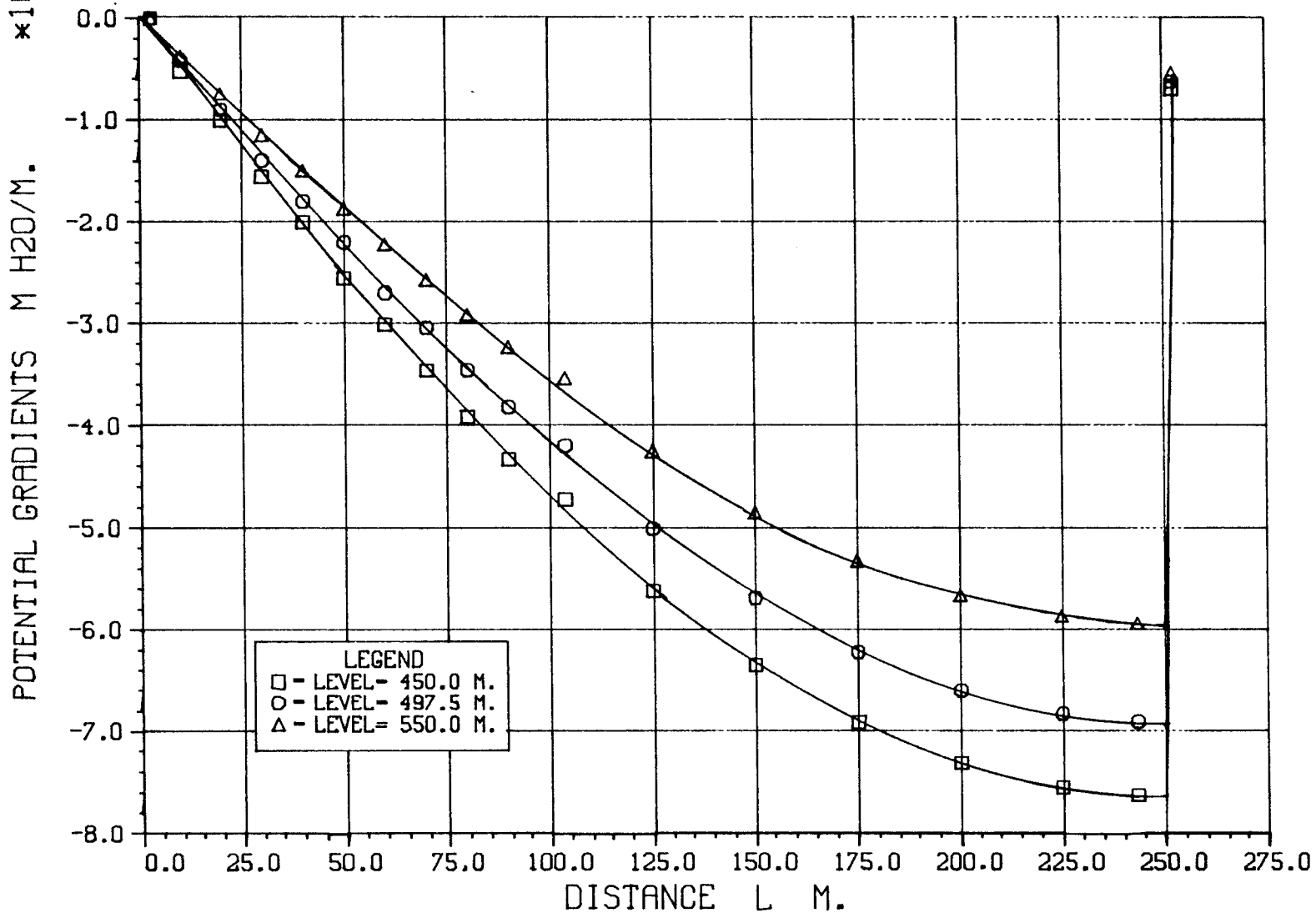

DIAGRAM NO: 7

POTENTIAL FIELD FROM WATER RIDGE.

VERTICAL POTENTIAL GRADIENTS AT VARIOUS LEVELS.

L(WR)-100 M, L(F)-250 M, Z(M)-3100 M, KP(F)-KP×(E+8)

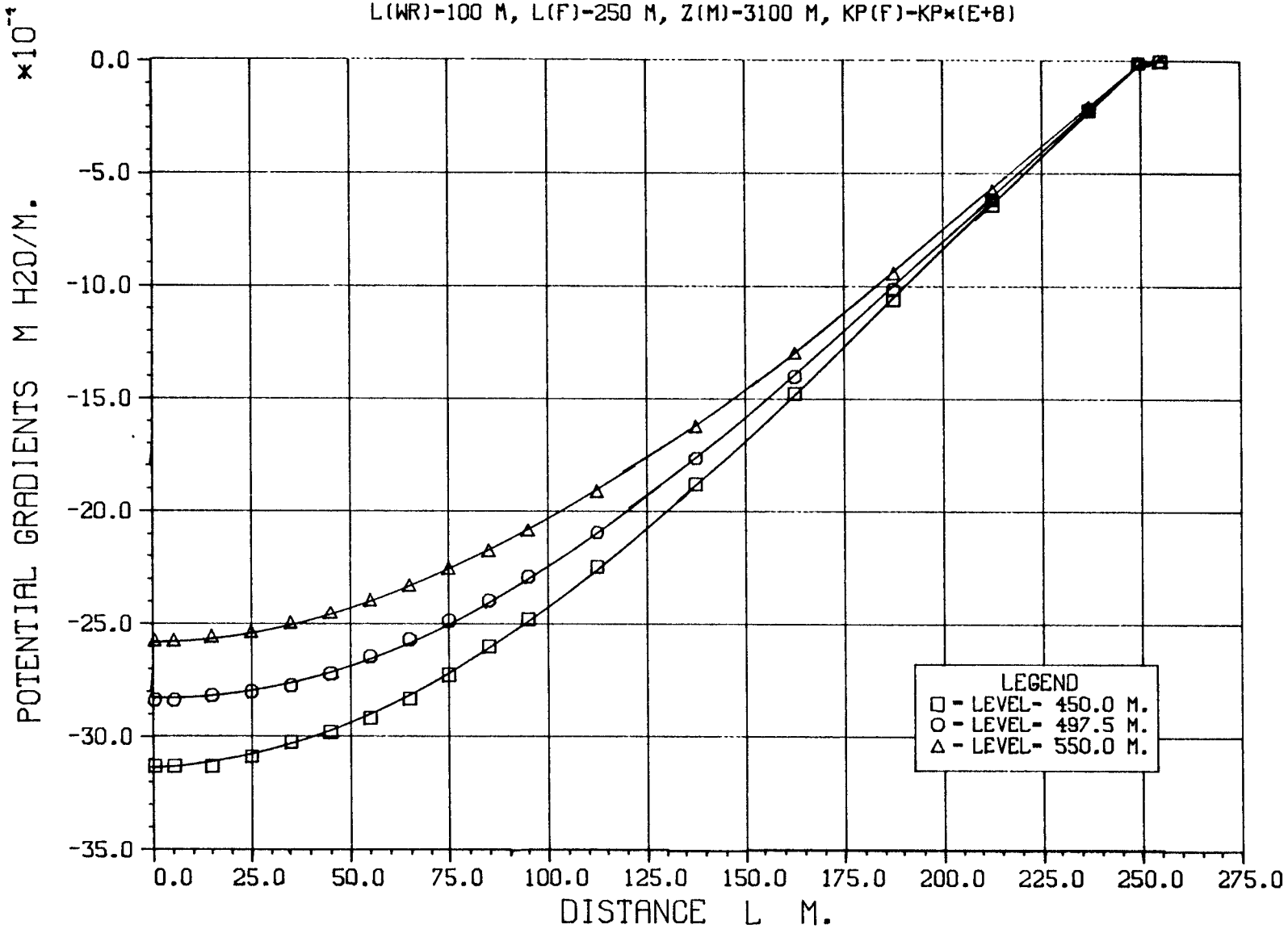

DIAGRAM NO: 8

DIAGRAM NO: 9

POTENTIAL FIELD FROM WATER RIDGE.

3D-DIAGRAM FOR POTENTIAL FIELD.

L(WR)-100 M, L(F)-250 M, Z(M)-3100 M, KP(F)-KP*(E+8)

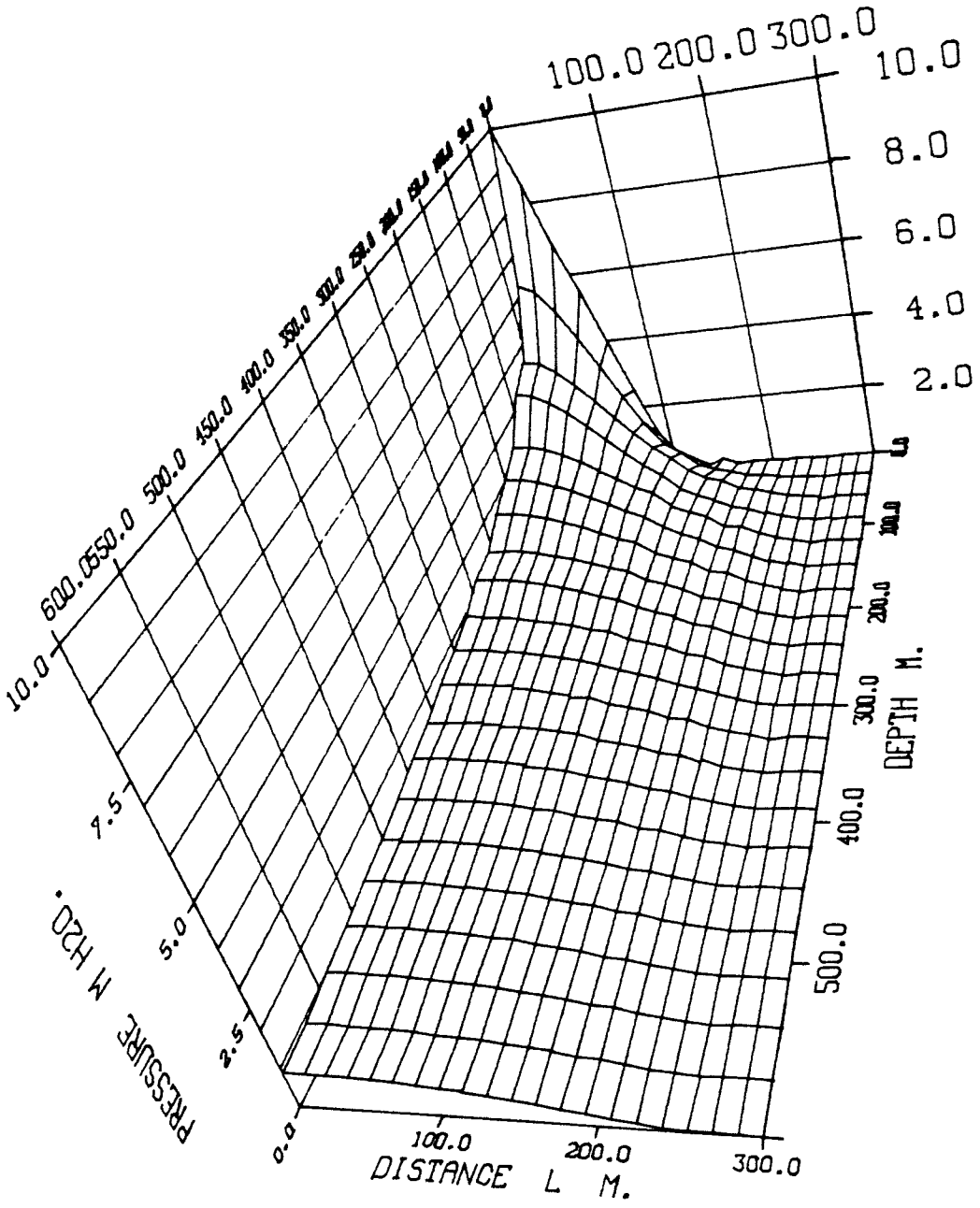

POTENTIAL FIELD FROM WATER RIDGE.

CONTOUR DIAGRAM OVER POTENTIAL FIELD.

L(WR)-100 M, L(F)-250 M, Z(M)-3100 M, KP(F)-KP*(E+8)

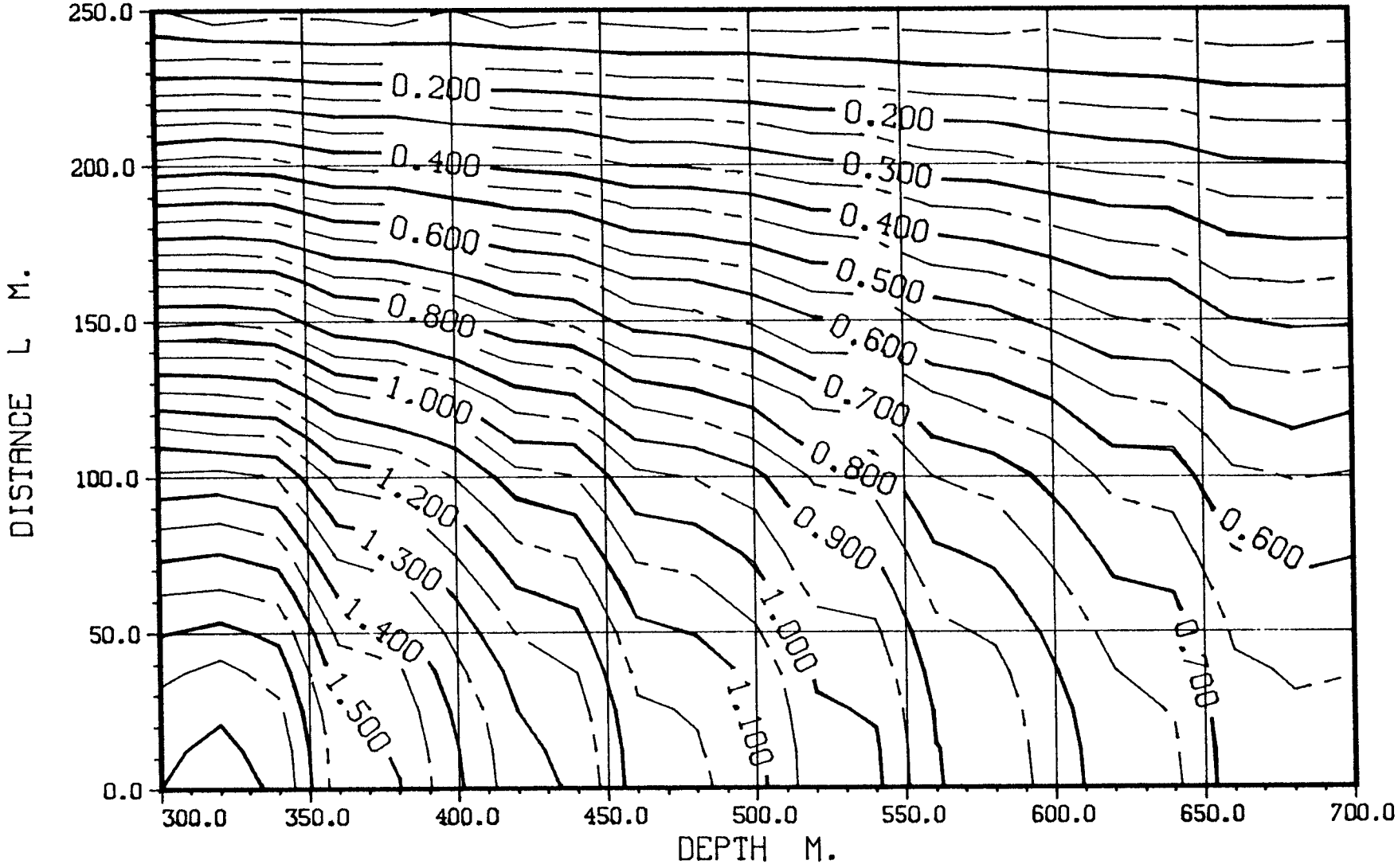

DIAGRAM NO: 10

DIAGRAM NO: 11

POTENTIAL FIELD FROM WATER HILL.

WATER HILL POTENTIALS AT VARIOUS LEVELS.

R(WH)-100 M, R(F)-250 M, Z(M)-3100 M, KP(F)-KP*100

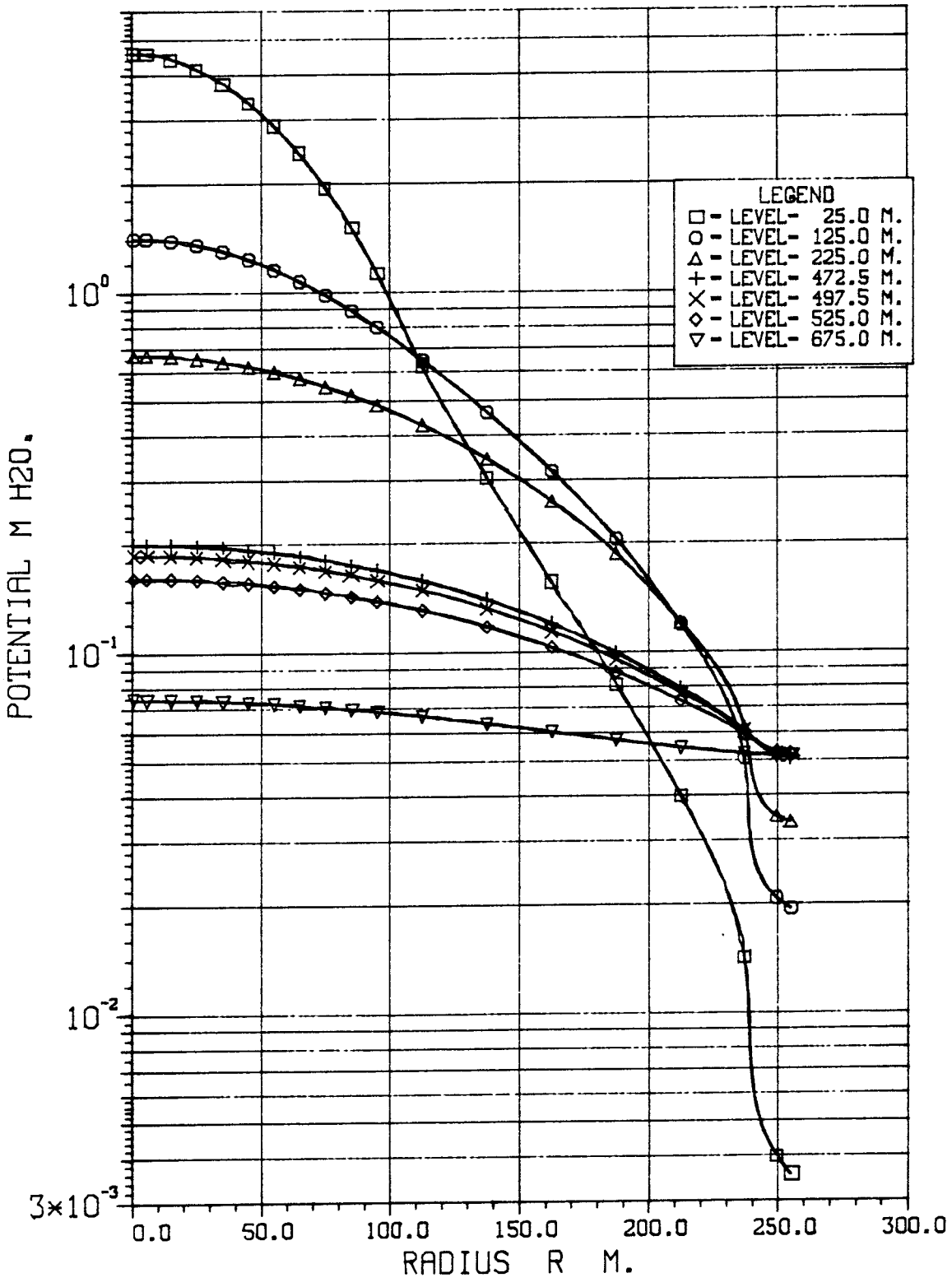

POTENTIAL FIELD FROM WATER HILL.

HORISONTAL POTENTIAL GRADIENTS AT VARIOUS LEVELS.

R(WH)-100 M, R(F)-250 M, Z(M)-3100 M, KP(F)-KP×100

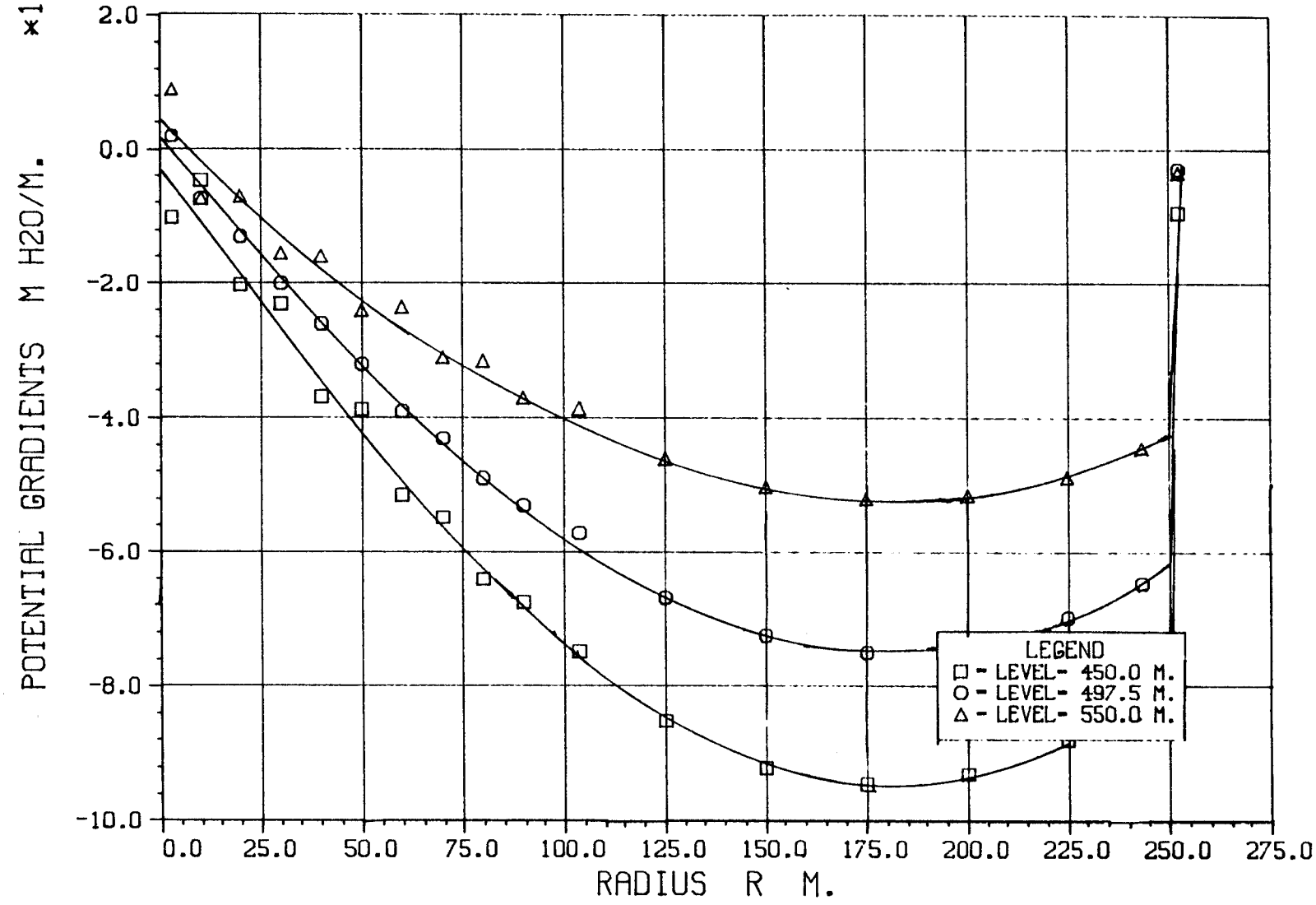

DIAGRAM NO: 12

POTENTIAL FIELD FROM WATER HILL.

VERTICAL POTENTIAL GRADIENTS AT VARIOUS LEVELS.

R(WH)-100 M, R(F)-250 M, Z(M)-3100 M, KP(F)-KP*100

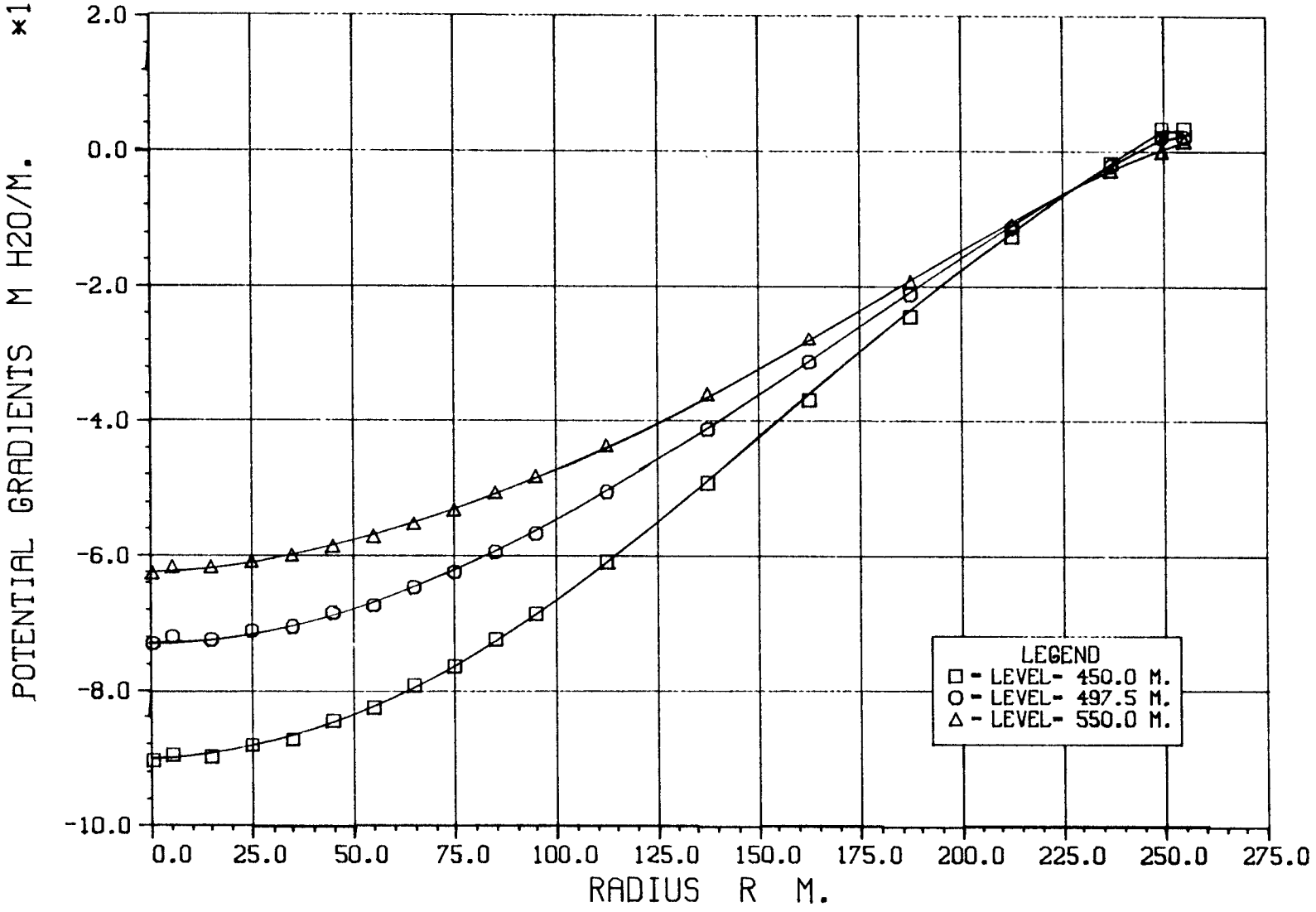

DIAGRAM NO: 13

DIAGRAM NO: 14

POTENTIAL FIELD FROM WATER HILL.

3D-DIAGRAM FOR POTENTIAL FIELD.

R(WH)-100 M, R(F)-250 M, Z(M)-3100 M, KP(F)-KP*100

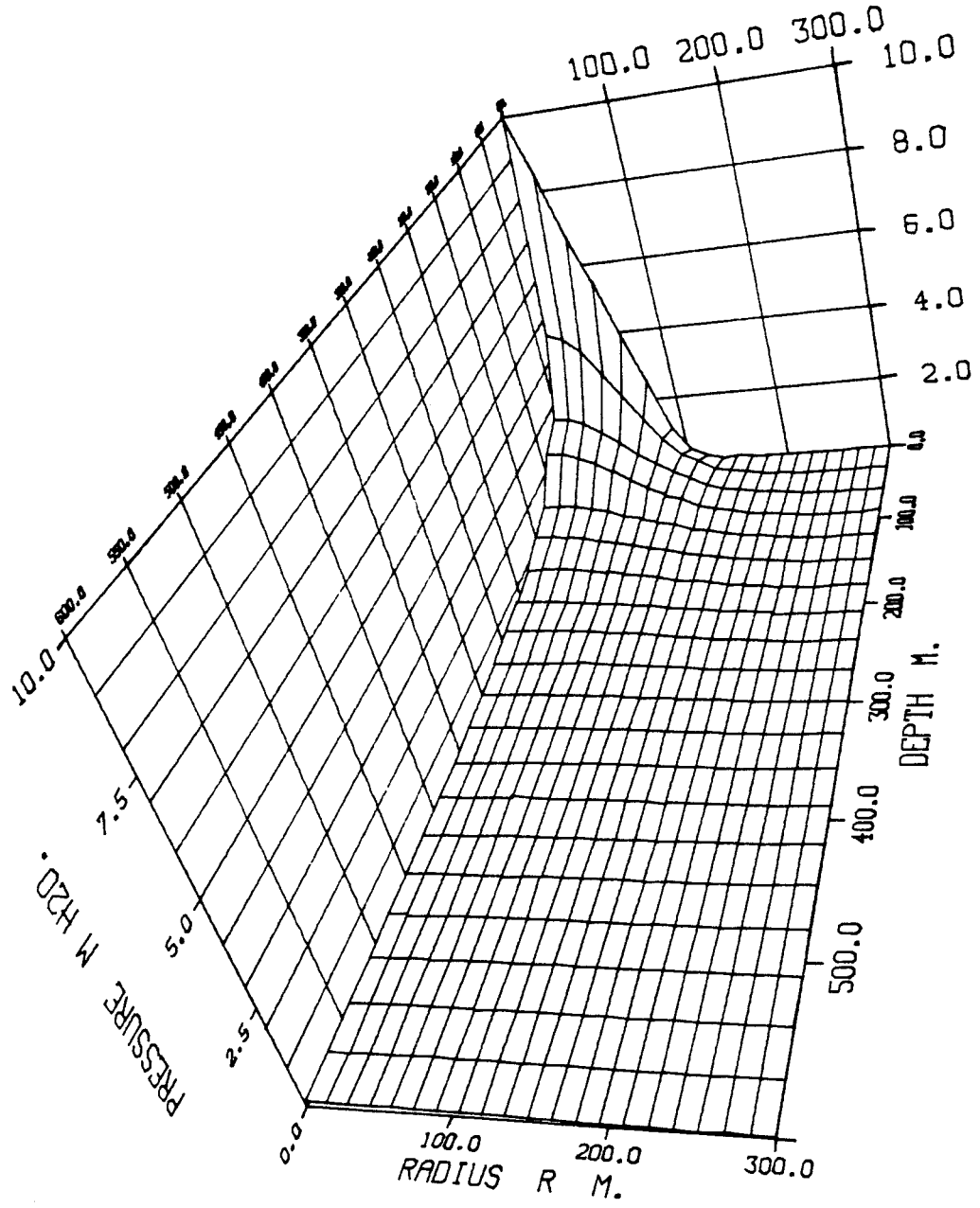

POTENTIAL FIELD FROM WATER HILL.

CONTOUR DIAGRAM OVER POTENTIAL FIELD.

R(WH)-100 M, R(F)-250 M, Z(M)-3100 M, KP(F)-KP*100

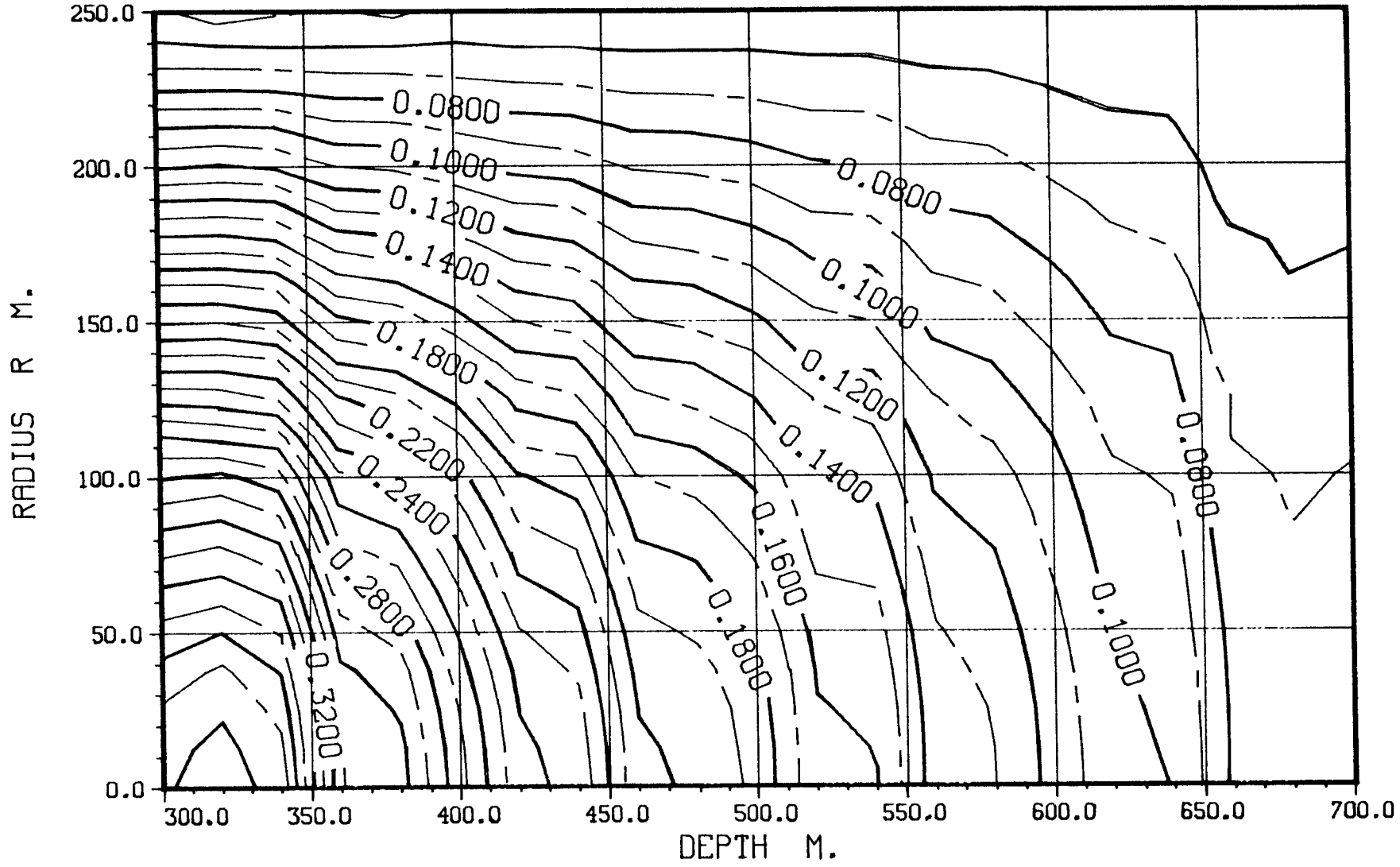

DIAGRAM NO: 15

DIAGRAM NO: 16

POTENTIAL FIELD FROM WATER HILL.

WATER HILL POTENTIALS AT VARIOUS LEVELS.

R(WH)-100 M, R(F)-250 M, Z(M)-3100 M, KP(F)-KP*(E+8)

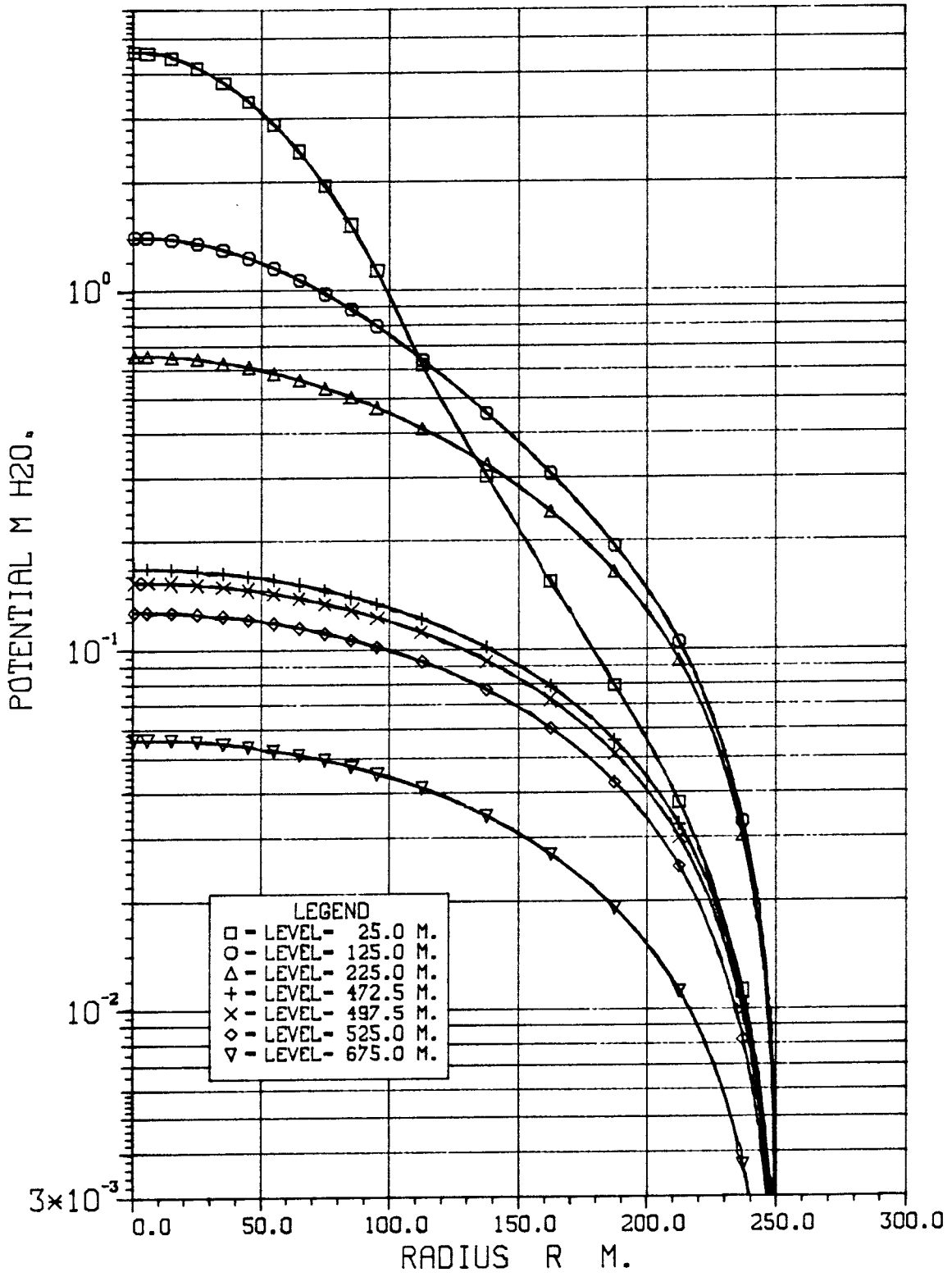

POTENTIAL FIELD FROM WATER HILL.

HORISONTAL POTENTIAL GRADIENTS AT VARIOUS LEVELS.

R(WH)-100 M, R(F)-250 M, Z(M)-3100 M, KP(F)-KP*(E+8)

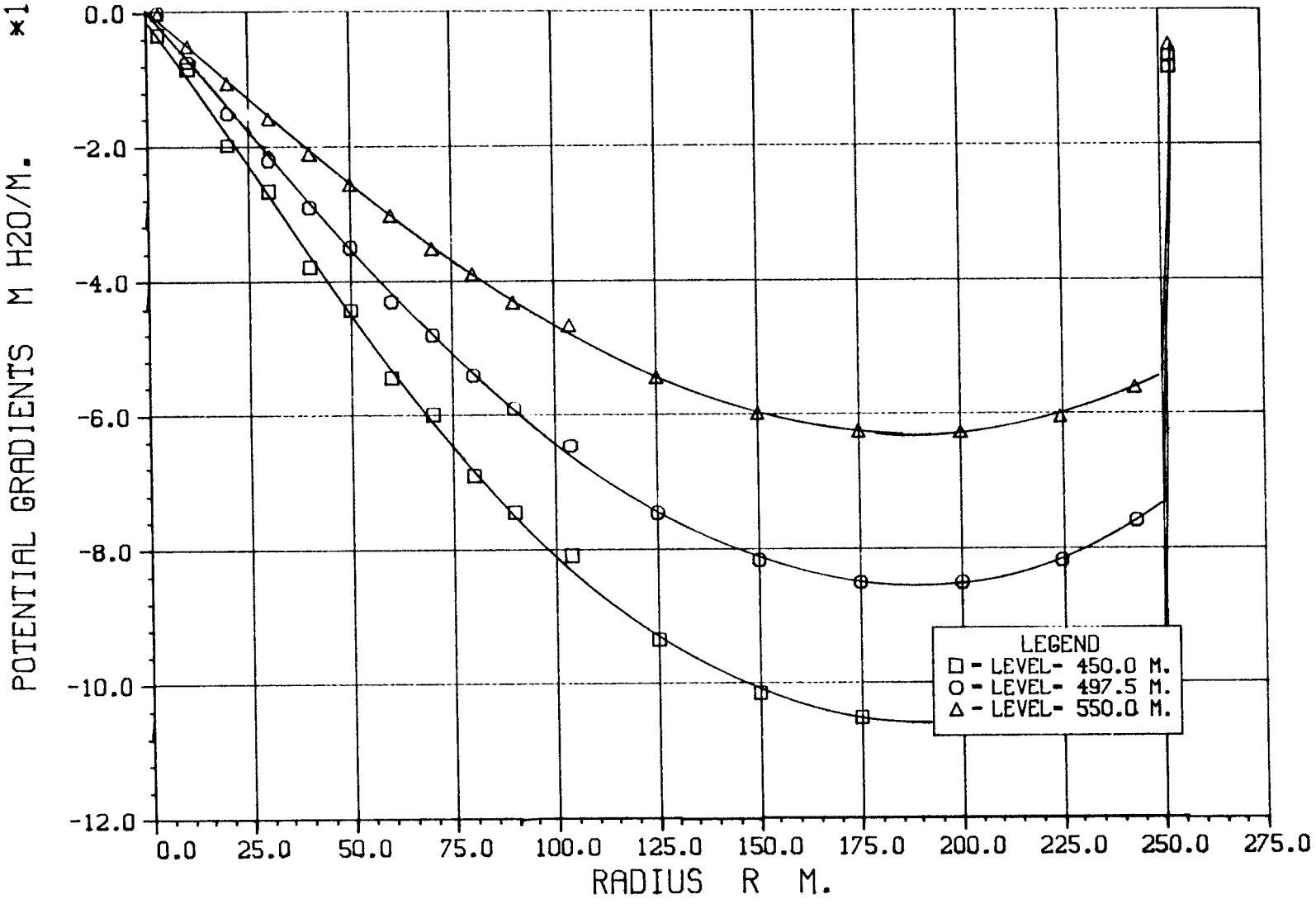

DIAGRAM NO: 17

POTENTIAL FIELD FROM WATER HILL.

VERTICAL POTENTIAL GRADIENTS AT VARIOUS LEVELS.

R(WH)-100 M, R(F)-250 M, Z(M)-3100 M, KP(F)-KP×(E+8)

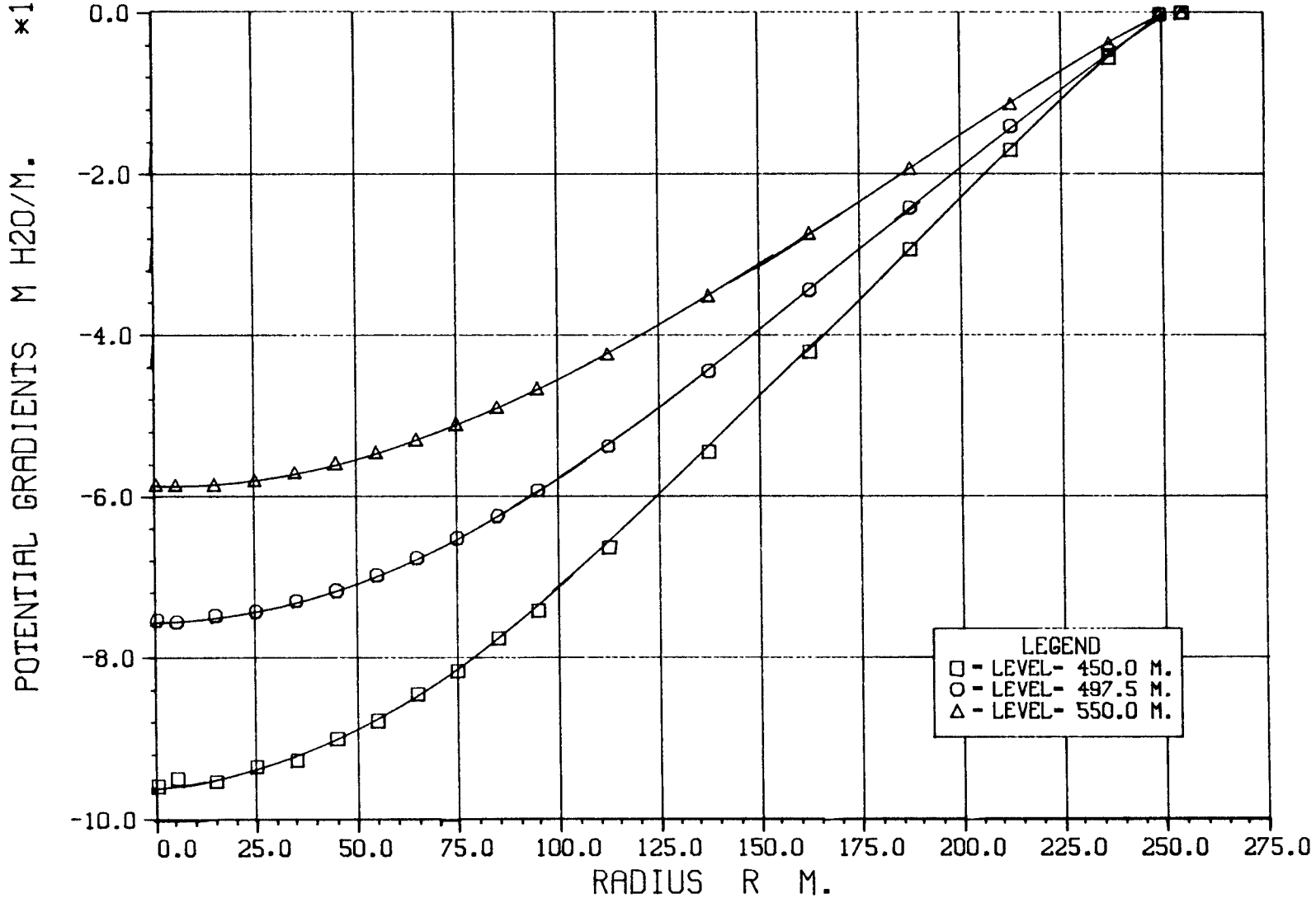

DIAGRAM NO: 18

DIAGRAM NO: 19

POTENTIAL FIELD FROM WATER HILL.

3D-DIAGRAM FOR POTENTIAL FIELD.

R(WH)-100 M, R(F)-250 M, Z(M)-3100 M, KP(F)-KP*(E+8)

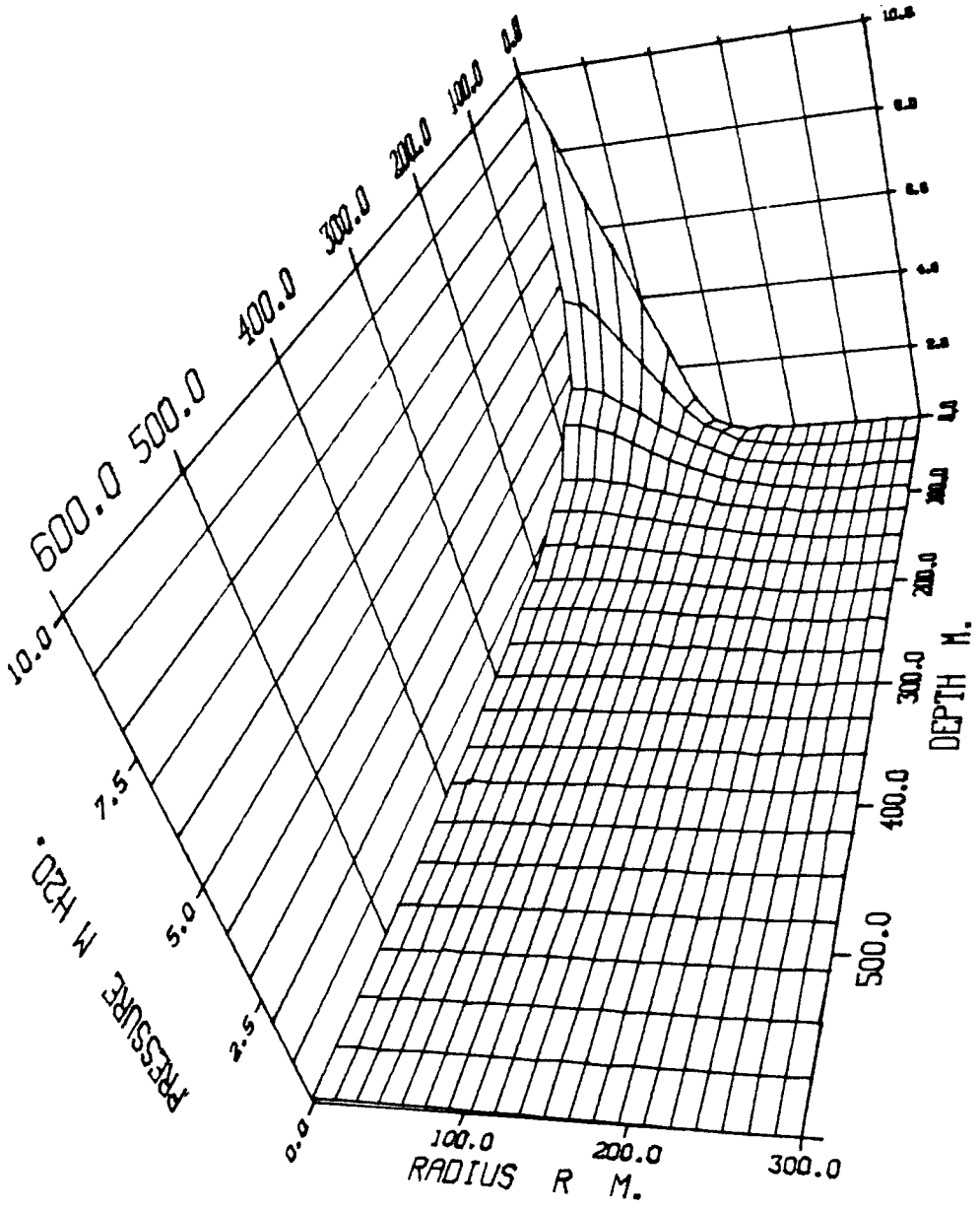

POTENTIAL FIELD FROM WATER HILL.

CONTOUR DIAGRAM OVER POTENTIAL FIELD.

R(WH)-100 M, R(F)-250 M, Z(M)-3100 M, KP(F)-KP×(E+8)

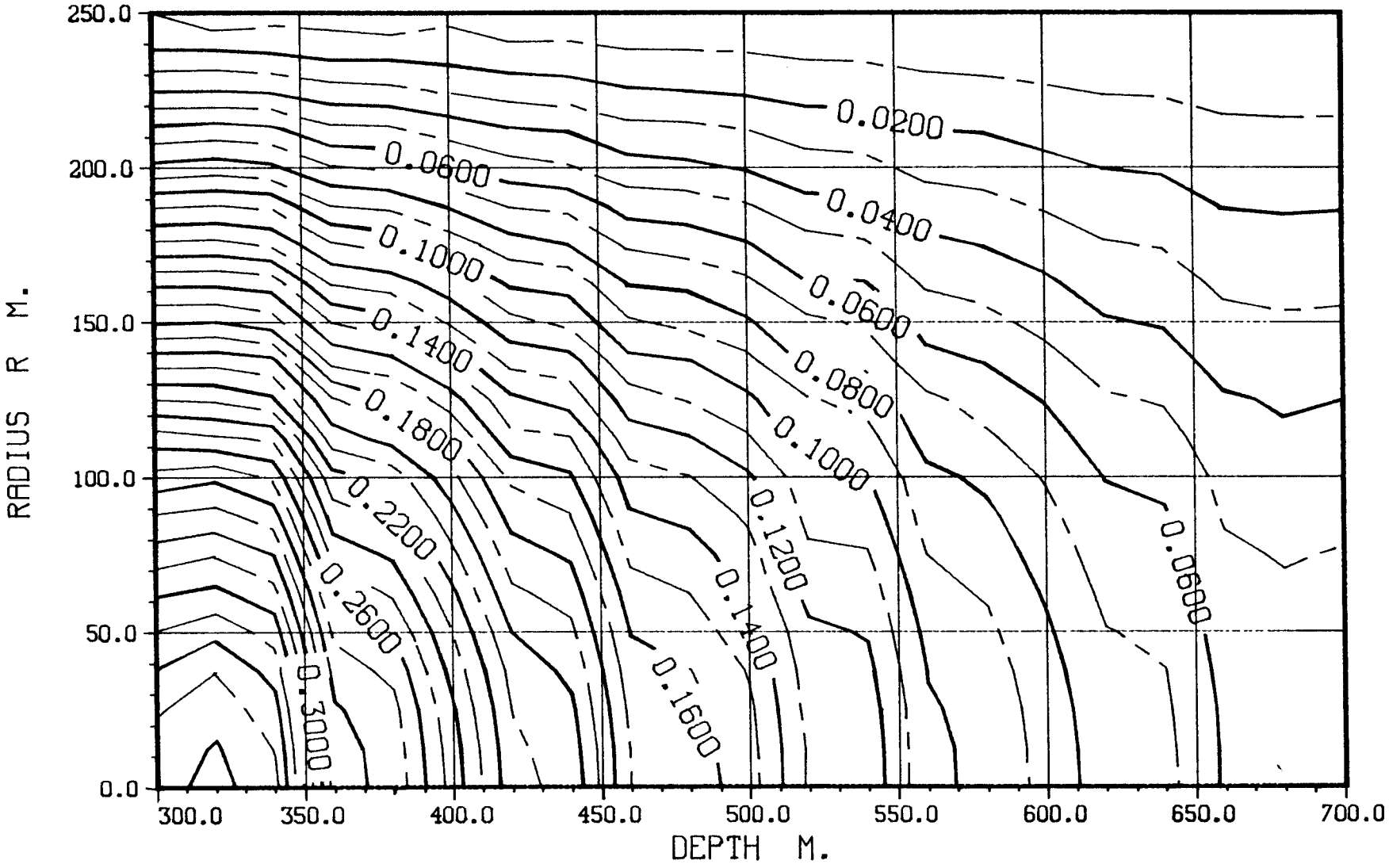

DIAGRAM NO: 20

LIST OF KBS's TECHNICAL REPORTS

1977-78

TR 121 KBS Technical Reports 1 - 120.
Summaries. Stockholm, May 1979.

1979

TR 79-28 The KBS Annual Report 1979.
KBS Technical Reports 79-01--79-27.
Summaries. Stockholm, March 1980.

1980

TR 80-26 The KBS Annual Report 1980.
KBS Technical Reports 80-01--80-25.
Summaries. Stockholm, March 1981.

1981

TR 81-17 The KBS Annual Report 1981.
KBS Technical Reports 81-01--81-16
Summaries. Stockholm, April 1982.

1983

TR 83-01 Radionuclide transport in a single fissure
A laboratory study
Trygve E Eriksen
Department of Nuclear Chemistry
The Royal Institute of Technology
Stockholm, Sweden 1983-01-19

TR 83-02 The possible effects of alfa and beta radiolysis on the matrix dissolution of spent nuclear fuel
I Grenthe
I Puigdomènech
J Bruno
Department of Inorganic Chemistry
Royal Institute of Technology
Stockholm, Sweden January 1983

TR 83-03 Smectite alteration
Proceedings of a colloquium at State University of New York at Buffalo, May 26-27, 1982
Compiled by Duwayne M Anderson
State University of New York at Buffalo
February 15, 1983

TR 83-04 Stability of bentonite gels in crystalline rock - Physical aspects
Roland Pusch
Division Soil Mechanics, University of Luleå
Luleå, Sweden, 1983-02-20

TR 83-05 Studies in pitting corrosion on archeological bronzes - Copper
Åke Bresle
Jozef Saers
Birgit Arrhenius
Archaeological Research Laboratory
University of Stockholm
Stockholm, Sweden 1983-01-02

TR 83-06 Investigation of the stress corrosion cracking of pure copper
L A Benjamin
D Hardie
R N Parkins
University of Newcastle upon Tyne
Department of Metallurgy and Engineering Materials
Newcastle upon Tyne, Great Britain, April 1983

TR 83-07 Sorption of radionuclides on geologic media - A literature survey. I: Fission Products
K Andersson
B Allard
Department of Nuclear Chemistry
Chalmers University of Technology
Göteborg, Sweden 1983-01-31

TR 83-08 Formation and properties of actinide colloids
U Olofsson
B Allard
M Bengtsson
B Torstenfelt
K Andersson
Department of Nuclear Chemistry
Chalmers University of Technology
Göteborg, Sweden 1983-01-30

TR 83-09 Complexes of actinides with naturally occurring organic substances - Literature survey
U Olofsson
B Allard
Department of Nucluear Chemistry
Chalmers University of Technology
Göteborg, Sweden 1983-02-15

TR 83-10 Radiolysis in nature:
Evidence from the Oklo natural reactors
David B Curtis
Alexander J Gancarz
New Mexico, USA February 1983

TR 83-11 Description of recipient areas related to final storage of unreprocessed spent nuclear fuel
Björn Sundblad
Ulla Bergström
Studsvik Energiteknik AB
Nyköping, Sweden 1983-02-07

TR 83-12 Calculation of activity content and related properties in PWR and BWR fuel using ORIGEN 2
Ove Edlund
Studsvik Energiteknik AB
Nyköping, Sweden 1983-03-07

TR 83-13 Sorption and diffusion studies of Cs and I in concrete
K Andersson
B Torstenfelt
B Allard
Department of Nuclear Chemistry
Chalmers University of Technology
Göteborg, Sweden 1983-01-15

TR 83-14 The complexation of Eu(III) by fulvic acid
J A Marinsky
State University of New York at Buffalo, Buffalo,NY
1983-03-31

TR 83-15 Diffusion measurements in crystalline rocks
Kristina Skagius
Ivars Neretnieks
Royal Institute of Technology
Stockholm, Sweden 1983-03-11

TR 83-16 Stability of deep-sited smectite minerals in crystalline rock - chemical aspects
Roland Pusch
Division of Soil Mechanics, University of Luleå
1983-03-30

TR 83-17 Analysis of groundwater from deep boreholes in
Gideå Sif Laurent
Swedish Environmental Research Institute
Stockholm, Sweden 1983-03-09

TR 83-18 Migration experiments in Studsvik
O Landström
Studsvik Energiteknik AB
C-E Klockars
O Persson
E-L Tullborg
S Å Larson
Swedish Geological
K Andersson
B Allard
B Torstenfelt
Chalmers University of Technology
1983-01-31

TR 83-19 Analysis of groundwater from deep boreholes in Fjällveden
Sif Laurent
Swedish Environmental Research Institute
Stockholm, Sweden 1983-03-29

TR 83-20 Encapsulation and handling of spent nuclear fuel for final disposal
1 Welded copper canisters
2 Pressed copper canisters (HIPOW)
3 BWR Channels in Concrete
B Lönnerberg, ASEA-ATOM
H Larker, ASEA
L Ageskog, VBB
May 1983

TR 83-21 An analysis of the conditions of gas migration from a low-level radioactive waste repository
C Braester
Israel Institute of Technology, Haifa, Israel
R Thunvik
Royal Institute of Technology
November 1982

TR 83-22 Calculated temperature field in and around a repository for spent nuclear fuel
Taivo Tarandi, VBB
Stockholm, Sweden April 1983

TR 83-23 Preparation of titanates and zeolites and their uses in radioactive waste management, particularly in the treatment of spent resins
Å Hultgren, editor
C Airola
Studsvik Energiteknik AB
S Forberg, Royal Institute of Technology
L Fälth, University of Lund
May 1983

TR 83-24 Corrosion resistance of a copper canister for spent nuclear fuel
The Swedish Corrosion Research Institute and its reference group
Stockholm, Sweden April 1983

TR 83-25 Feasibility study of EB welding of spent nuclear fuel canisters
A Sanderson, T F Szluha, J Turner
Welding Institute
Cambridge, United Kingdom April 1983

TR 83-26 The KBS UO_2 leaching program
Summary Report 1983-02-01
Ronald Forsyth, Studsvik Energiteknik AB
Nyköping, Sweden February 1983

TR 83-27 Radiation effects on the chemical environment in a radioactive waste repository
Trygve Eriksen
Royal Institute of Technology, Stockholm
Arvid Jacobsson
University of Luleå, Luleå
Sweden 1983-07-01

TR 83-28 An analysis of selected parameters for the BIOPATH-program
U Bergström
A-B Wilkens
Studsvik Energiteknik AB
Nyköping, Sweden 1983-06-08

TR 83-29 On the environmental impact of a repository for spent nuclear fuel
Otto Brotzen
Stockholm, Sweden April 1983

TR 83-30 Encapsulation of spent nuclear fuel - Safety Analysis
ES-konsult AB
Stockholm, Sweden April 1983

TR 83-31 Final disposal of spent nuclear fuel - Standard programme for site investigations
Compiled by
Ulf Thoregren
Swedish Geological
April 1983

TR 83-32 Feasibility study of detection of defects in thick welded copper
Tekniska Röntgencentralen AB
Stockholm, Sweden April 1983

TR 83-33 The interaction of bentonite and glass with aqueous media
M Mosslehi
A Lambrosa
J A Marinsky
State University of New York
Buffalo, NY, USA April 1983

TR 83-34 Radionuclide diffusion and mobilities in compacted bentonite
B Torstenfelt
B Allard
K Andersson
H Kipatsi
L Eliasson
U Olofsson
H Persson
Chalmers University of Technology
Göteborg, Sweden April 1983

TR 83-35 Actinide solution equilibria and solubilities in geologic systems
B Allard
Chalmers University of Technology
Göteborg, Sweden 1983-04-10

TR 83-36 Iron content and reducing capacity of granites and bentonite
B Torstenfelt
B Allard
W Johansson
T Ittner
Chalmers University of Technology
Göteborg, Sweden April 1983

TR 83-37 Surface migration in sorption processes
A Rasmuson
I Neretnieks
Royal Institute of Technology
Stockholm, Sweden March 1983

TR 83-38 Evaluation of some tracer tests in the granitic rock at Finnsjön
L Moreno
I Neretnieks
Royal Institute of Technology, Stockholm
C-E Klockars
Swedish Geological, Uppsala
April 1983

TR 83-39 Diffusion in the matrix of granitic rock
Field test in the Stripa mine. Part 2
L Birgersson
I Neretnieks
Royal Institute of Technology
Stockholm, Sweden March 1983

TR 83-40 Redox conditions in groundwaters from Svartboberget, Gideå, Fjällveden and Kamlunge
P Wikberg
I Grenthe
K Axelsen
Royal Institute of Technology
Stockholm, Sweden 1983-05-10

TR 83-41 Analysis of groundwater from deep boreholes in Svartboberget
Sif Laurent
Swedish Environmental Research Institute
Stockholm, Sweden 1983-06-10

TR 83-42 Final disposal of high-level waste and spent nuclear fuel - foreign activities
R Gelin
Studsvik Energiteknik AB
Nyköping, Sweden May 1983

TR 83-43 Final disposal of spent nuclear fuel - geological, hydrological and geophysical methods for site characterization
K Ahlbom
L Carlsson
O Olsson
Swedish Geological
Sweden May 1983

TR 83-44 Final disposal of spent nuclear fuel - equipment for site characterization
K Almén, K Hansson, B-E Johansson, G Nilsson
Swedish Geological
O Andersson, IPA-Konsult
P Wikberg, Royal Institute of Technology
H Åhagen, SKBF/KBS
May 1983

TR 83-45 Model calculations of the groundwater flow at Finnsjön, Fjällveden, Gideå and Kamlunge
L Carlsson
A Winberg
Swedish Geological, Göteborg
B Grundfelt
Kemakta Consultant Company, Stockholm
May 1983

TR 83-46 Use of clays as buffers in radioactive repositories
Roland Pusch
University of Luleå
Luleå May 25 1983

TR 83-47 Stress/strain/time properties of highly compacted bentonite
Roland Pusch
University of Luleå
Luleå May 1983

TR 83-48 Model calculations of the migration of radionuclides from a repository for spent nuclear fuel
A Bengtsson
Kemakta Consultant Company, Stockholm
M Magnusson
I Neretnieks
A Rasmuson
Royal Institute of Technology, Stockholm
May 1983

TR 83-49 Dose and dose commitment calculations from groundwaterborne radioactive elements released from a repository for spent nuclear fuel
U Bergström
Studsvik Energiteknik AB
Nyköping, Sweden May 1983

TR 83-50 Calculation of fluxes through a repository caused by a local well
R Thunvik
Royal Institute of Technology
Stockholm, Sweden May 1983

TR 83-51 GWHRT - A finite element solution to the coupled ground water flow and heat transport problem in three dimensions
B Grundfelt
Kemakta Consultant Company
Stockholm, Sweden May 1983

TR 83-52 Evaluation of the geological, geophysical and hydrogeological conditions at Fjällveden
K Ahlbom
L Carlsson
L-E Carlsten
O Duran
N-Å Larsson
O Olsson
Swedish Geological
May 1983

TR 83-53 Evaluation of the geological, geophysical and hydrogeological conditions at Gideå
K Ahlbom
B Albino
L Carlsson
G Nilsson
O Olsson
L Stenberg
H Timje
Swedish Geological
May 1983

TR 83-54 Evaluation of the geological, geophysical and hydrogeological conditions at Kamlunge
K Ahlbom
B Albino
L Carlsson
J Danielsson
G Nilsson
O Olsson
S Sehlstedt
V Stejskal
L Stenberg
Swedish Geological
May 1983

TR 83-55 Evaluation of the geological, geophysical and hydrogeological conditions at Svartboberget
K Ahlbom
L Carlsson
B Gentzschein
A Jämtlid
O Olsson
S Tirén
Swedish Geological
May 1983

TR 83-56 I: Evaluation of the hydrogeological conditions at Finnsjön
II: Supplementary geophysical investigations of the Sternö peninsula
B Hesselström
L Carlsson
G Gidlund
Swedish Geological
May 1983

TR 83-57 Neotectonics in northern Sweden - geophysical investigations
H Henkel
K Hult
L Eriksson
Geological Survey of Sweden
L Johansson
Swedish Geological
May 1983

TR 83-58 Neotectonics in northern Sweden - geological investigations
R Lagerbäck
F Witschard
Geological Survey of Sweden
May 1983

TR 83-59 Chemistry of deep groundwaters from granitic bedrock
B Allard
Chalmers University of Technology
S Å Larson
E-L Tullborg
Swedish Geological
P Wikberg
Royal Institute of Technology
May 1983

TR 83-60 On the solubility of technetium in geochemical systems
B Allard
B Torstenfelt
Chalmers University of Technology
Göteborg, Sweden 1983-05-05

TR 83-61 Sorption behaviour of well-defined oxidation states
B Allard
U Olofsson
B Torstenfelt
H Kipatsi
Chalmers University of Technology
Göteborg, Sweden 1983-05-15

TR 83-62 The distribution coefficient concept and aspects on experimental distribution studies
B Allard
K Andersson
B Torstenfelt
Chalmers University of Technology
Göteborg, Sweden May 1983

TR 83-63 Sorption of radionuclides in geologic systems
K Andersson
B Torstenfelt
B Allard
Chalmers University of Technology
Göteborg, Sweden 1983-06-15

TR 83-64 Ion exchange capacities and surface areas of some major components and common fracture filling materials of igneous rocks
B Allard
M Karlsson
Chalmers University of Technology
E-L Tullborg
S Å Larson
Swedish Geological
Göteborg, Sweden May 1983

TR 83-65 Sorption of actinides on uranium dioxide and zirconium dioxide in connection with leaching of uranium dioxide fuel
B Allard
N Berner
K Andersson
U Olofsson
B Torstenfelt
Chalmers University of Technology
R Forsyth
Studsvik Energiteknik AB
May 1983

TR 83-66 The movement of radionuclides past a redox front
I Neretnieks
B Åslund
Royal Institute of Technology
Stockholm, Sweden 1983-04-22

TR 83-67 Some notes in connection with the studies of final disposal of spent fuel. Part 2
I Neretnieks
Royal Institute of Technology
Stockholm, Sweden May 1983

TR 83-68 Two dimensional movements of a redox front downstream from a repository for nuclear waste
I Neretnieks
B Åslund
Royal Institute of Technology
Stockholm, Sweden 1983-06-03

TR 83-69 An approach to modelling radionuclide migration in a medium with strongly varying velocity and block sizes along the flow path
I Neretnieks
A Rasmuson
Royal Institute of Technology
Stockholm, Sweden May 1983

TR 83-70 Analysis of groundwater from deep boreholes in Kamlunge
S Laurent
Swedish Environmental Research Institute
Stockholm, Sweden May 1983

TR 83-71 Gas migration through bentonite clay
Roland Pusch
Thomas Forsberg
University of Luleå
Luleå, Sweden May 31, 1983